

ALOS-2 PALSAR-2 L-band cross-polarized radar data analysis for modelling above-ground biomass/carbon stock and carbon sequestration of tropical rainforest, Berkelah, Malaysia

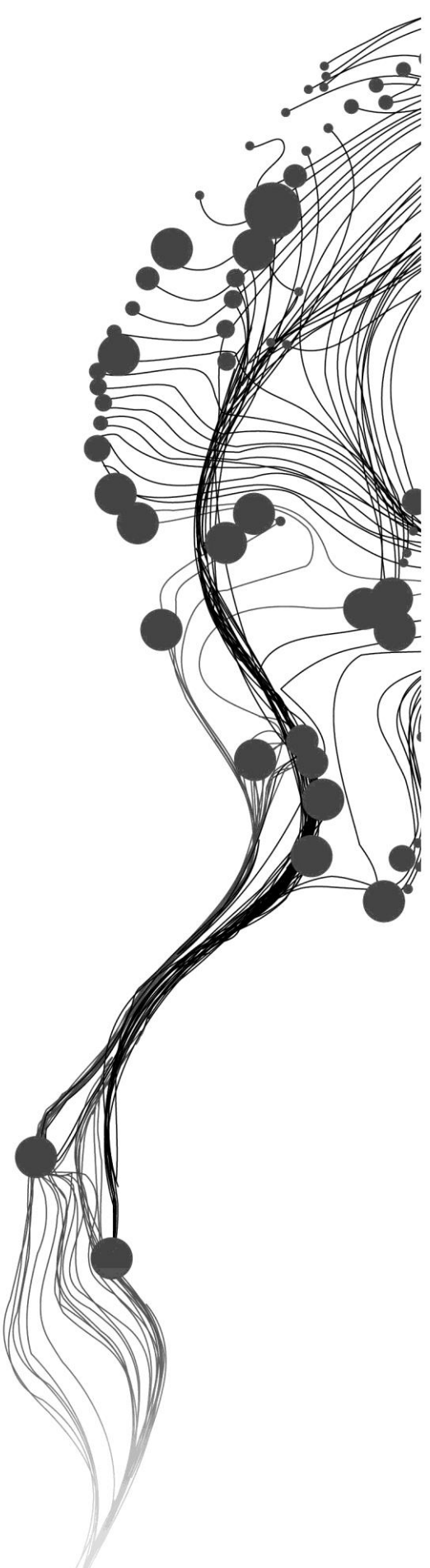
ROBERT NAGABONA MASOLELE

February 2018

SUPERVISORS:

Dr. Yousif A. Hussin

Drs. E. H. Kloosterman



ALOS-2 PALSAR-2 L-band cross-polarized radar data analysis for modelling above-ground biomass/carbon stock and carbon sequestration of tropical rainforest, Berkelah, Malaysia

ROBERT NAGABONA MASOLELE

Enschede, The Netherlands, February 2017

Thesis submitted to the Faculty of Geo-Information Science and Earth Observation of the University of Twente in partial fulfilment of the requirements for the degree of Master of Science in Geo-information Science and Earth Observation.

Specialization: Natural Resources Management

SUPERVISORS:

Dr. Yousif A. Hussin

Drs.E.H. Kloosterman

ADVISOR

Dr. Zulkiflee Abd Latif

THESIS ASSESSMENT BOARD:

Prof.dr. A.D. Nelson (Chair)

Dr. T. Kauranne (External Examiner, LUT school of Engineering Science, Finland)

DISCLAIMER

This document describes work undertaken as part of a programme of study at the Faculty of Geo-Information Science and Earth Observation of the University of Twente. All views and opinions expressed therein remain the sole responsibility of the author, and do not necessarily represent those of the Faculty.

ABSTRACT

In this thesis research, we examined the application of L-band ALOS-2 PALSAR-2 SAR data to model the AGB/carbon stock and carbon sequestration of the tropical rainforest. The SAR parameters were evaluated on the basis of the single SAR backscatter image, time series analysis of SAR backscatter, together with an analysis of the influence of combined HV, HH backscatter on AGB estimation. Also, the Saturation effect of radar backscatter for AGB estimation was established by determining the saturation level at which AGB prediction tend to level off. The seasonal (Moist, Dry) dependence of SAR backscatter for AGB estimation were also analysed. The satellite SAR data used for this study were represented by a time series of SAR images acquired in three-time periods of the years September- 2006, January-2017 and September 2017 by the ALOS-2 PALSAR-2 sensor. The study area is in the tropical rainforest Berkelah-Malaysia and represented a typical managed complex tropical rainforest land. Relationship of different L-band SAR parameters, their temporal stability was studied along with reference field AGB data calculated from forest DBH and tree height measurements. Further, two polarimetric parameters, cross-polarisation and co-polarization backscatter, were chosen for further investigation and AGB retrieval.

A relationship between forest AGB and L-band SAR parameters were established using the linear, logarithmic, and Multiple regression approaches. Ways of obtaining the optimal combination of L-band SAR images were evaluated as well. For a single scene, the best results were observed with HV-polarized backscatter ($R^2 \approx 0.82$, $RMSE \approx 79\text{tons ha}^{-1}$) and ($R^2 \approx 0.87$, $RMSE \approx 68\text{tons ha}^{-1}$) using logarithmic regression for scenes acquired in September - 2016 and September - 2017 conditions respectively. SAR backscatter saturation was estimated at 270tons ha^{-1} , the point at which SAR backscatter response to AGB started to decrease by 0.02dB. At the same time, AGB validation result with an ($R^2 \approx 0.8$, $RMSE \approx 84\text{tons ha}^{-1}$) and ($R^2 \approx 0.78$, $RMSE \approx 88\text{tons ha}^{-1}$) was achieved for logarithmic and linear regression analysis of HV backscatter respectively. Hence, logarithmic regression was a better predictor of AGB than using linear regression. Multiple aggregations of HV, HH did not significantly improve the AGB estimates for both studied SAR parameters with p-value >0.05 . The stronger achievement was observed in the estimation of the amount of carbon sequestration between September 2016 to September 2017. An estimated total of 3.62tons ha^{-1} of carbon was sequestered in Berkelah forest in one year. This study proved that combining temporal series of SAR scenes could be a better estimator of carbon sequestration.

On the relationship between forest height from L-band interferometry and LiDAR, an ($R^2 \approx 0.56$, $RMSE \approx 4\text{m}$) was obtained. Finally, the backscatter distribution in the study area was studied using the tomographic slice in the azimuth direction. Backscatter contribution to AGB estimates was observed to come from both ground and forest canopy, most of the high-power backscatter was detected to come from the ground floor $<10\text{m}$ height, indicating that there is an influence of ground signal to backscatter relationship with forest AGB.

In general L-band, SAR backscatter has proved to have a significant potential for AGB/carbon stock estimation and carbon sequestration. It provides an opportunity for climate change programs (REDD+) to engage more in using SAR data for forest carbon monitoring. However, challenges of SAR backscatter saturation, moisture effect on SAR backscatter and accurate forest height estimation for AGB estimation using SAR data, still need to be addressed.

Keywords: Aboveground biomass, Synthetic Aperture Radar, Interferometry, Tomography, Tropical forests.

ACKNOWLEDGEMENTS

My first acknowledgement goes to the Almighty God for allowing me to exist in this world and his protection with all the adversaries. Without him, nothing of this thesis could have been accomplished.

It is also, with great honour to give thanks to the University of Twente, Faculty of geo-information science and earth observation (ITC), for giving me an opportunity morally and financially to pursue the MSc program. The opportunity has enabled me to acquire skills and knowledge in GIS and RS that will have an enormous impact on my career. I kindly give thanks to my first supervisor Dr. Yousif Ali Hussin for his tireless, continuous advice, comments, and support during the entire research period. Also, to my second supervisor Drs. E. Henk Kloosterman for his tireless support and dedication during the research period, particularly during fieldwork data collection in the Berkelah tropical rain forest, Malaysia.

It is my great pleasure also to thank the NRM course director Drs. RG. Nijmeijer, for his advice, support and smooth coordination of the coursework, thesis modules and thesis defence. He is indeed a good leader; I am very grateful to have him as my course director.

Also, my gratitude goes to the University of Technology Mara Malaysia (UiTM), especially Associate Professor Sr Dr. Zulkiflee Abd Latif and Ms. Syaza Rozali, PhD Candidates, for their hospitality and support during the field work in Malaysia. They helped in arranging fieldwork logistics, and they also supported us with transport from Kuala Lumpur to where the field area was located and return transport to Kuala Lumpur.

I would also like to thank my fieldwork colleagues, Ms. Belinda Odia, Mr. A.N. Wassihun, Mr. T.H. Berhe, Mr. Solomon Begashaw and Mr. Exavery Kigosi for their participation and cooperation during the fieldwork. As without their support the data collection work would have been a difficult task to handle alone.

Lastly, my humble appreciation goes to my beloved wife Janeth William Kasubi, my lovely children Hendrick and Ellen Masolele for their lovely, moral support and comfort for me to achieve my dreams. Also, my heartfelt gratitude goes to the rest of my family, my mother Avila Magessa, my father Thomas Masolele. They have been great well-wishers in the hardest time and by putting me in their prayers. Without their support, the road to writing this thesis would not have been easy.

Robert Nagabona Masolele

Enschede, The Netherlands

February 2018

TABLE OF CONTENTS

LIST OF FIGURES.....	vii
LIST OF TABLES.....	ix
LIST OF EQUATIONS.....	x
LIST OF APPENDICES.....	xi
LIST OF ACRONYMS.....	xii
1. INTRODUCTION.....	1
1.1. Background.....	1
1.2. Problem statement and justification.....	2
1.3. Research objectives.....	3
1.3.1. General objective.....	3
1.3.2. Specific objectives.....	3
1.3.3. Research questions.....	4
1.3.4. Research hypothesis.....	4
1.3.5. Concepts of the study.....	4
2. LITERATURE REVIEW.....	6
2.1. Synthetic aperture radar.....	6
2.2. SAR interferometry.....	7
2.3. SAR tomography.....	8
2.4. Laser scanners (LiDAR).....	9
2.4.1. Airborne laser scanner (ALS).....	9
2.4.2. Terrestrial laser scanner (TLS).....	10
3. STUDY AREA, MATERIALS, AND METHODS.....	11
3.1. Study area.....	11
3.1.1. Geographical location.....	11
3.1.2. Vegetation type and topography.....	11
3.1.3. Climate.....	11
3.2. Materials.....	12
3.2.1. Field equipment's and data.....	12

3.2.2. Software	12
3.3. Research methods	13
3.4. Field work	14
3.4.1. Field sampling design	14
3.4.2. Determining plot size	15
3.5. Data collection.....	15
3.5.1. Biometric data collection	15
3.5.2. Data collection with TLS	16
3.5.3. ALS data acquisition	16
3.5.4. Alos-2-Palsar-2 SAR data acquisition	16
3.6. Data processing and analysis.....	17
3.6.1. Terrestrial laser scanner data processing	17
3.6.2. Airborne laser scanner data processing	17
3.6.3. ALOS-2 PALSAR-2 SAR data pre-processing for backscatter retrieval.....	19
3.6.4. Retrieval of radar backscatter coefficient and radiometric correction.....	19
3.6.5. Above-ground biomass saturation point estimation	21
3.6.6. Retrieval of radar backscatter coefficients for time series analysis of AGB/carbon stock and carbon sequestration	21
3.6.7. Multiple logarithmic regression analysis of AGB and L-band HV, HH polarised radar backscatter in relation to single HV backscatter.....	22
3.6.8. ALOS-2 PALSAR-2 SAR interferometry processing	23
3.6.9. Tomographical retrieval of backscatter distribution.....	27
3.6.10. Above-ground biomass calculation.....	27
3.7. Statistical analysis	28
3.7.1. The relationship between AGB and L-band cross polarised radar backscatters	28
3.7.2. Estimation of the backscatter saturation point	28
3.7.3. The relationship of AGB, time series L-band cross polarised radar backscatters and carbon stock sequestration.....	28
3.7.4. The relationship between interferometric height and LiDAR height.....	28
3.7.5. The tomographic distribution of L-band cross polarised radar backscatters in relation to AGB ...	28
3.7.6. Above-ground biomass (AGB) and carbon stock estimation and mapping	28

4.	RESULTS	29
4.1.	Statistical analysis of field data.....	29
4.2.	Statistical analysis of HV radar backscatter.....	30
4.3.	The relationship between AGB and L-band cross polarised radar backscatters.....	31
4.4.	The saturation point of the above-ground biomass in relation to L-band cross polarised radar backscatters	33
4.5.	Model validation and accuracy assessment.....	33
4.5.1.	Validation data.....	33
4.5.2.	Model validation and accuracy assessment	33
4.6.	The relationship between AGB and time series of L-band polarised radar backscatters, and its influence on carbon stock sequestration estimation.....	34
4.7.	The relationship between AGB and a combined L-band HV, HH polarised radar backscatter in relation to single HV backscatter.....	36
4.8.	Interferometric height results	36
4.8.1.	The relationship between LiDAR-derived CHM height and radar-derived CHM height	38
4.9.	Tomographic distribution of the L-band cross polarised radar backscatters in relation to AGB.....	38
4.9.1.	Vertical distribution of HV backscatter in relation to height estimated from DEM differencing algorithm	39
4.10.	Estimated AGB and carbon stock of the study area	40
5.	DISCUSSION.....	41
5.1.	The Relationship between AGB and L-band cross polarized radar backscatters	41
5.2.	Biomass saturation.....	42
5.3.	The Relationship between AGB and time series of L-band polarized backscatters and its influence on carbon stock sequestration estimation.....	44
5.4.	The relationship between AGB and a combined L-band HV, HH polarised radar backscatter in relation to single HV backscatter.....	45
5.5.	The relationship between interferometric forest height and LiDAR forest height.....	45
5.6.	The relationship between tomographic backscatter layers and AGB	46
5.7.	The research relevance for REDD+	47
5.8.	Study limitations.....	47
6.	CONCLUSION.....	48
6.1.	Conclusion	48

6.2. Recommendation..... 49
LIST OF REFERENCES..... 51

LIST OF FIGURES

Figure 1: The conceptual diagram of the study	5
Figure 2: Scattering contribution from the forest.....	7
Figure 3: Interferometric imaging geometry.....	8
Figure 4: 3D imaging of the forest structure.....	8
Figure 5: Generation of multilayer SAR images from multi baseline SAR images	9
Figure 6: Acquisition geometry of LiDAR remote sensing.....	10
Figure 7: Map of the study area of Berkelah Rain Forest in Kuantan District, Malaysia.	11
Figure 8: Flowchart of the research method	14
Figure 9: Multiple scans.	16
Figure 10: LiDAR digital surface model.	18
Figure 11: The SAR image acquisition geometry of topographical distortions.....	19
Figure 12: Raw SAR image as compared to backscatter image.....	20
Figure 13: Backscatter retrieval from cross-polarized backscatter coefficient SAR image.....	21
Figure 14: The map of subset area used for estimation of carbon sequestration between the year September 2016 and September 2017.....	22
Figure 15: HH Interferometric coherence and phase of the study area.	24
Figure 16: HV Interferometric coherence and phase of the study area.....	24
Figure 17: Images of flattened and filtered interferogram for HH and HV polarised SAR images.	25
Figure 18: Interferometric vertical wavenumber of the study area derived from SAR images.....	25
Figure 19: The Height variations of the study area derived from SAR images using DEM differencing forest height inversion algorithms.	26
Figure 20: Density and Histogram plots showing the distribution of AGB in the Study Area.....	29
Figure 21: The density plot, the frequency distribution of backscatters and vertical distribution of backscatters in height direction.	30
Figure 22: Scatter plot of the correlation between the cross-polarised backscatter and the Above Ground Biomass.	31
Figure 23: The scatter plot of the regression line between the cross-polarised backscatter and the above-ground biomass..	32
Figure 24: The graph showing the AGB saturation point with respect to the SAR backscatter. The red vertical line intersecting the AGB axis shows the estimated saturation point (slope=0.02dB).....	33

Figure 25: The scatter plots to check model validity, the predicted AGB on the y-axis and observed AGB on the x-axis.	34
Figure 26: The scatter plots of the regression line between the september 2016 cross-polarised backscatter values and the above-ground biomass.....	34
Figure 27: Carbon stock of the subset study area for the year september 2016/ 2017 and the corresponding sequestered carbon.....	35
Figure 28: (c) and (d) Height profile line and its residuals drawn over (a) LiDAR CHM (b) Radar CHM derived by use of DEM differencing algorithm.....	37
Figure 29: A scatter plot showing the SAR interferometric height distribution in relation to height derived from LiDAR data.....	38
Figure 30: Vertical tomographic slice.....	39
Figure 31: Scatter plot of the HV backscatter distribution in relation to DEM differencing interferometric height.....	39
Figure 32: Distribution of AGB and carbon stock in the study area as of september 2016.....	40
Figure 33: Distribution of AGB and carbon stock in the study area as of september 2017.....	40
Figure 34. The scatter plot of the logarithmic regression of AGB and ALOS PALSAR L-band HV polarisation by Hamdan et al. (2011) in tropical rainforest of Malaysia.....	42
Figure 35. From Mitchard et al. (2009) ALOS PALSAR (a) HH and (b) HV backscatter in 4 locations of African tropical forest in which radar backscatter plotted against field-measured AGB (Mg/ha) for all four sites combined, with the x-axes shown with conventional and log10 scales.....	42
Figure 36: L-band backscatter saturation at lower AGB values.....	43
Figure 37: Temporal backscatter distribution from the field plots.....	45
Figure 38: Coherence phase variation in the study area.....	45
Figure 39: A quantitative comparison of ALOS InSAR inverted height and LiDAR height.....	46
Figure 40: Azimuth tomographic slice through canopy.....	47

LIST OF TABLES

Table 1: List of field equipment's, data and their purpose	12
Table 2: List of software's and their purpose.....	12
Table 3: SAR parameters and models used for time-series analysis for AGB/carbon stock sequestration.....	22
Table 4: Summary statistics of forest parameters.	29
Table 5: Summary statistics of the linear regression model of AGB and HV backscatters.....	31
Table 6: Summary statistics of the logarithmic regression model of AGB and HV backscatters.	32
Table 7: Summary statistics of the logarithmic regression model of AGB and time series of cross polarised radar image of September 2016.	35
Table 8: The average amount of AGB/Carbon stock from the subset and the sequestered carbon.....	35
Table 9: Summary statistics of the multiple logarithmic regression model of AGB and HV, HH polarised radar backscatter.....	36
Table 10: Comparison of the cross polarised radar backscatter logarithmic regression model and multiple logarithmic regression model of the cross and like polarised radar backscatter.	36

LIST OF EQUATIONS

Equation 1: Equation for retrieval of backscatter coefficient	20
Equation 2: Equation for determining the AGB saturation point.....	21
Equation 3: Multiple logarithmic equation AGB and HV, HH polarised backscatter	22
Equation 4: Equation for Interferogram Generation.....	23
Equation 5: Equation for generating the flattened interferogram	24
Equation 6: Equation for calculating the vertical wavenumber.....	25
Equation 7: DEM differencing algorithm	26
Equation 8: Fourier transform	27
Equation 9: Backscattered power distribution.....	27
Equation 10: Allometric equation	27
Equation 11: Carbon equation	28
Equation 12: Inverted logarithmic equation for AGB estimation.....	32

LIST OF APPENDICES

Appendix 1: Field data collection sheet	57
Appendix 2: Statistical summary output of regression results	58
Appendix 3: Results of the linear and logarithmic regression between AGB and HV backscatter for the 28 January 2017 backscatter image.	59
Appendix 4: ALOS-2 PALSAR-2 SAR image footprint as viewed in Google Earth	59
Appendix 5: Average monthly rainfall pattern over the year in Kuantan, Malaysia.....	60
Appendix 6: Backscatter images of September 2016, January 2017 and September 2017 for Berkelah tropical rain forest, Malaysia.....	61

LIST OF ACRONYMS

AGB	Above Ground Biomass
ALOS-2	Advanced Land Observation Satellite-2
ALS	Aerial Laser Scanner
BA	Basal Area
DBH	Diameter at Breast Height
FAO	Food and Agriculture Organization
GIS	Geographic Information System
HH	Horizontal send, Horizontal receive
HV	Horizontal send, Vertical receive
IPCC	International Panel on Climate Change
ITC	Faculty of Geo-Information Science and Earth Observation
JAXA	Japan Aerospace Exploration Agency
LiDAR	Light Detection And Ranging
MRV	Monitoring Reporting and Verification
PALSAR	Phased Array Synthetic Looking Aperture Radar-2
PoSARpro	Polarimetric SAR Data Processing and Educational Tool
RADAR	Radio Detection And Ranging
REDD+	Reduce Emission from Deforestation and Degradation Measurement
RS	Remote Sensing
SAR	Synthetic Aperture Radar
SNAP	Sentinels Application Platform 2
TLS	Terrestrial Laser Scanner
UNFCC	United Nation Framework Convention on Climate Change
UN-REDD	United Nation- Reduce Emission from Deforestation and Degradation
UTM	Universal Transverse Mercator

1. INTRODUCTION

1.1. Background

Forests cover represents 1/3 of the earth's surface (FAO, 2005). Primarily, tropical rain forests play a significant role in global climate change, through their unique nature of carbon sequestration, which regulates the worldwide as well as local temperatures (Djomo *et al.*, 2017). By taking into account only tropical regions, deforestation accounts for up to 20% of the carbon dioxide emitted by human activities each year (Ho Tong Minh *et al.*, 2014). Thus, on accounting to reduce emission from tropical forest, the United National Framework Convention on Climate Change developed a program known as REDD+ to contribute to reducing the emissions from deforestation and forest degradation. The mechanism creates a financial value as an incentive to the parties, particularly developing countries which reduce carbon emission from forests (FAO, 2017).

Based on REDD+, the developing countries can reduce emissions from deforestation and forest degradation, by implementing either sustainable forest management, avoiding deforestation, avoiding forest degradation, forest conservation or by enhancing forest carbon stock (FAO, 2017). To be able to claim the financial benefit for reduced emission, the parties are required to present the proof of increased biomass/carbon stock in their forests. To achieve that several methods have been proposed to quantify the change in forest biomass/carbon stock (The REDD Desk, 2017).

Measuring Reporting and Verification (MRV) is the mechanism that REDD+ program is proposing to all parties, for which it recommends the use of different remote sensing techniques such as very high-resolution satellite images, SAR images (backscatter) and LiDAR to assess above-ground biomass and carbon stock (FFPRI, 2012).

Above ground biomass (AGB) is one of the larger global carbon pool and it has an impact on the ecology and earth's climate system (FAO Climate Energy and Tenure Division, 2009). Making it an important parameter to monitor for changes in atmospheric carbon dioxide (Lucas *et al.*, 2015). There are various methods for AGB/carbon stock estimation, ranging from destructive measurement to nondestructive measurement which involves the use of allometric equations, use of remote sensing data and forest growth models (Lucas *et al.*, 2015). The destructive measurements for biomass estimation have reasonable accuracies (Gibbs *et al.*, 2007). However, the high cost, labour requirement and time, limit its application on a larger scale, making the non-destructive method using remote sensing data the best suitable practical option to predict AGB on more major scales forest with reasonable effort (Villard *et al.*, 2016).

Remote sensing data ranging from optical to active have been used for AGB/carbon stock estimation for some decades (Lucas *et al.*, 2015). However, the active sensors (LiDAR and Radar) are said to have high accuracy in estimating AGB/carbon stock (Gibbs *et al.*, 2007). This is due to their ability to derive the forest parameters, such as forest stand and trees height, diameter at breast height(DBH) and forest volume (Caicoya *et al.*, 2015; Joshi *et al.*, 2015; Kaasalainen *et al.*, 2015; Sarker *et al.*, 2012). While passive sensors which utilise the canopy visible and IR reflections, vegetation indices have been used as proxies for AGB/carbon stock (Lu *et al.*, 2004; Powell *et al.*, 2010).

LiDAR provides high accurate tree height, and DBH measurements for AGB estimation thus considered the most accurate sensor for AGB estimation (Rahman *et al.*, 2017; Strahler *et al.*, 2008). However, LiDAR data availability are limited by acquisition from an airborne laser scanner or a Terrestrial laser scanner (Liang *et al.*,

2016; Rahman *et al.*, 2017). Thus, its applications are restricted due to small area coverage, the high cost of operations and cloud cover free conditions requirement (Gibbs *et al.*, 2007). Unlike LiDAR, Radar system below x-band frequencies are not hampered by cloud cover or other effects like fog or haze; they provide continuous earth coverage for monitoring forests trend and other environmental factors (Hong Tong Minh *et al.*, 2012; Omar *et al.*, 2015; Villard *et al.*, 2016). The Radar wavelength bands L and P are key for AGB estimation, as their backscatters are related to tree trunks and branches volume scattering which contribute to total forest biomass (Villard *et al.*, 2016).

This study, therefore, sets out to model above-ground biomass/carbon stock and estimate the carbon sequestration, using L-band cross polarised ALOS-2 PALSAR-2 satellite data along with Laser Scanner data in a tropical rain forest of Berkelah, Malaysia. The study explores the possibility of obtaining a highly accurate model which can best predict the above ground biomass/carbon stock. Estimate carbon sequestration. Estimate forest height from L-band ALOS-2 PALSAR-2 SAR images by interferometry analysis and assess the effect of vertical backscatter distribution for accuracy of AGB/Carbon stock estimation using SAR tomography analysis.

1.2. Problem statement and justification

REDD+ proposes the need for an accurate Measuring, Reporting and Verification (MRV) system for AGB (Gibbs *et al.*, 2007), this increases the demand for a model, to accurately and precisely predict the above-ground biomass in various forest ecosystems.

The ALOS-2 L-band cross polarised PalSAR backscatter data have been used satisfactorily for AGB/carbon stock estimation, due to a reasonable correlation that exists between its backscatter values and the AGB/carbon stock (Odipo *et al.*, 2016; Sumareke, 2016). However, due to the density and structure of tropical forests, the use of radar backscatter to retrieve AGB/carbon stock is challenging, and it leads to AGB underestimation (Ho Tong Minh *et al.*, 2014; Hong Tong Minh *et al.*, 2012; Villard *et al.*, 2016). L-band radar can estimate tropical forests AGB up to 150 tons per ha and tend to saturate with high AGB >150 tons/ha (Villard *et al.*, 2016). The main reason for the under-estimation of AGB/carbon stock being the decrease in intensity sensitivity of the radar backscatter, also known as saturation effect (Ho Tong Minh *et al.*, 2014; Hong Tong Minh *et al.*, 2012). For this reason, different images processing techniques such as SAR tomography have been developed and used to exploit the 3D backscatter power distribution of radar signals to reduce the SAR saturation effect and hence increase the amount of AGB estimation (Ho Tong Minh *et al.*, 2014).

Few studies, specifically in tropical forests has been done to identify the saturation point of backscatter for AGB Estimation (Hamdan *et al.*, 2015; Imhoff, 1995; Mermoz *et al.*, 2014; Mermoz *et al.*, 2015). Thus, it becomes challenging to answer questions like; at which AGB values the relation between AGB and SAR backscatter can no longer be derived? Knowing clearly the maximum point at which backscatter can be used to model AGB, will be of great advantage to developing AGB models based on forest density and structure. Also, it will help in identifying the best time of the year for which the corresponding SAR data can be used to estimate AGB.

Advanced SAR image processing technique, such as the use of SAR tomography, has shown to reduce the saturation effect of radar images for AGB estimation (Mermoz *et al.*, 2014). By increasing the accuracy and quantity of AGB estimation as well as the prediction power of radar data (Chehade *et al.*, 2016; Ho Tong Minh *et al.*, 2014, 2015; Kumar *et al.*, 2017; Li *et al.*, 2015). AGB can be estimated by considering not only the

backscattered values at each slant range and azimuth location but also its vertical distribution by generating vertical layers at different heights preferably the height associated with forest volume backscatter, then retrieve these height layers backscatter for AGB estimation (Ho Tong Minh *et al.*, 2014). However, the challenge with this approach is the number of images required to achieve a desired baseline for retrieval of vertical forest structure.

LiDAR has proven to have reasonable accuracy and precise measurement to estimate AGB/carbon stock (Strahler *et al.*, 2008). By acquiring forest structure attributes, such as tree height and diameter at breast height, as opposed to the traditional data collection method (Mengesha *et al.*, 2015). However, AGB/carbon stock estimation over large forest area with LiDAR is very expensive and can be difficult to afford. In this study, Interferometric analysis using inversion algorithms was used to estimate the forest height parameter and compare it to LiDAR estimated forest height, then assess the potential application of height estimated by SAR data for AGB/carbon stock mapping.

Most studies on AGB/carbon stock estimation in tropical forests has been done using optical images (Du *et al.*, 2012; Dube & Mutanga, 2015; Gibbs *et al.*, 2007; Lu *et al.*, 2004; Powell *et al.*, 2010). However, tropical forests are affected by cloud condition in most of the year, making it difficult to obtain clear passive optical satellite images (Asner, 2001). Also, the use of optical sensors leads to underestimation of AGB and carbon stocks due to a dense canopy of tropical rainforest (Gibbs *et al.*, 2007). SAR is an active sensor which can be used in all-weather conditions, making it more reliable for accurate estimation of AGB/carbon stock (Omar *et al.*, 2015). However, few studies have been done to estimate AGB/carbon stock and especially carbon sequestration in tropical forestry using a combination of LiDAR and SAR data (Fan *et al.*, 1998). Therefore, this study was done specifically in estimating AGB/carbon stock and carbon sequestration using backscatter values, estimating forest height from L-band ALOS-2 PALSAR-2 SAR images using interferometry analysis and assessing the effect of vertical backscatter distribution for the accuracy of AGB/Carbon stock estimation.

1.3. Research objectives

1.3.1. General objective

This study is aiming at the analysis of L-band cross polarised ALOS-2 PALSAR-2 backscatter values, interferometric analysis and tomographic analysis along with terrestrial laser scanner and airborne laser scanner data for modelling above-ground biomass/carbon stock and carbon sequestration in a tropical rain forest of Berkelah, Malaysia.

1.3.2. Specific objectives

1. To analyse the relationship between AGB/carbon stock derived from (TLS and ALS) data, and L-band cross polarised radar backscatter values.
2. To determine the AGB Saturation point in relation to the L-band cross polarised radar backscatter values.
3. To determine the relationship between time series of the L-band cross polarised radar backscatters and AGB. Then estimate the carbon sequestered in the berkelah tropical rain forest in the period of one year 9/2016 to 9/2017.
4. To estimate forest height from interferometric SAR images of ALOS-2 PALSAR-2 and assess its relationship with ALS height.

5. To assess the tomographic distribution of the L-band cross polarised radar backscatters in height direction in relation to AGB.
6. To Estimate and map AGB/carbon stock by the L-band cross polarised radar backscatter.

1.3.3. Research questions

1. What is the relationship between L-band cross polarised radar backscatter values and AGB/carbon stock from TLS and ALS data?
2. What is the Saturation point of AGB estimation in relation to the L-band cross polarised radar backscatter values?
3. What is the relationship between time series of the L-band cross polarised radar backscatters and AGB? And how much carbon was sequestered in the berkelah tropical rain forest in 2016/2017?
4. What is the relationship between forest height estimated from interferometric SAR images of ALOS-2 PALSAR-2 and ALS height?
5. What is the distribution of the L-band cross polarised radar backscatters in height direction in relation to AGB?
6. What is the AGB/carbon stock estimated by L-band cross polarised radar backscatter image?

1.3.4. Research hypothesis

1. Ho: There is no significant relationship between AGB/carbon stock from TLS, ALS and L-band cross polarised radar backscatter.
Ha: There is a significant relationship between AGB/carbon stock from TLS, ALS and L-band cross polarised radar backscatter values.
2. Ho: There is no effect on L-band cross polarised radar backscatter saturation in AGB estimation.
Ha: There is an effect on L-band cross polarised radar backscatter saturation in AGB estimation.
3. Ho: There is no significant relationship between AGB/carbon stock from TLS, ALS and the time series of L-band polarised radar backscatters.
Ha: There is a significant relationship between AGB/carbon stock from TLS, ALS and the time series of L-band polarised radar backscatters.
4. Ho: There is no significant difference between forest trees height estimated by interferometric analysis and LiDAR data.
Ha: There is a significant difference between forest trees height estimated by interferometric analysis and LiDAR data.

1.3.5. Concepts of the study

The berkelah tropical rain forest is an important area for biomass/carbon stock, as it regulates climate change effect by sequestering carbon dioxide from the atmosphere. On the other hand, it also contributes to climate change through deforestation and forest degradation which are sources of increased carbon emissions.

Remote sensing is one of the main MRV systems for modelling AGB/carbon stock including VHRS optical images, LiDAR and SAR systems; but each system has limitations (FFPRI, 2012). In this study, we focused on SAR as the best alternative active remote sensing for AGB/carbon MRV system because of its characteristics: more extensive area coverage, a sensor for all weather conditions, and it is low-cost. The primary limitation posed by SAR data for AGB/carbon stock estimation using backscatter is saturation. In this study, we assessed the saturation problem by detecting the saturation point. Also, we used an image processing technique (SAR tomography) to determine the source of reflected backscatter power distribution of the SAR image and its effect on AGB/carbon modelling. Apart from that, time series of the L-band cross polarised radar backscatter was used to determine its relationship with AGB and estimate the carbon sequestered by the forest between September 2016/2017. Also, the interferometric analysis was done to retrieve the forest height parameter. The concept of the study is further illustrated in Figure 1.

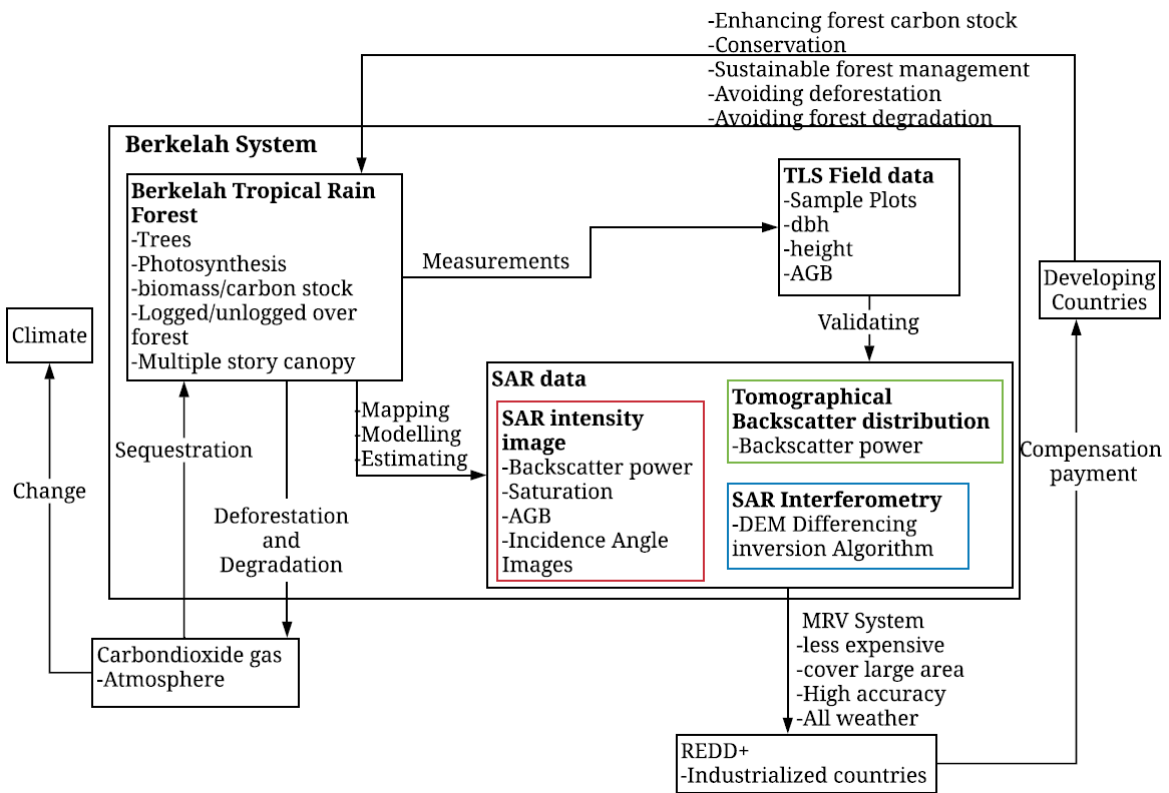


Figure 1: The conceptual diagram of the study

2. LITERATURE REVIEW

2.1. Synthetic aperture radar

SAR or Synthetic Aperture Radar is a type of radar sensor that has been widely used to monitor land surfaces due to its characteristics of using its own illumination energy, penetration of earth superficial materials, night imaging and all-weather imaging capability (Moreira *et al.*, 2013). SAR as an active sensor is a side looking system: It transmits electromagnetic pulses as it moves along its path and sequentially records the backscattered signal. The received backscatter results in the detection of object and determination of its position. Also, the range between the SAR antenna and the object is determined using the travel time of the received pulse (Ager, 2011).

Three factors affect the radar return signals: the system parameters, topography (slope and aspect) and characteristics of surface materials, which includes geometric properties of the object, e.g., surface roughness and dielectric properties of the object, e.g., moisture content (Moreira *et al.*, 2013). The system parameters are wavelength, polarisation and incidence angle. These parameters determine information retrieved from the SAR image. SAR has wavelength band ranges from a shorter wavelength to longer wavelength in order of X, C, S, L, P. The polarisation parameter has four combinations recognised as the HV, VH, HH and VV. The incidence angles range from near to far incidence angles (Ager, 2011). The three parameters determine the penetration of radar signals to various earth features and their scattering property, the object feature characteristics in an image, as well as information which can be derived from the SAR image (Moreira *et al.*, 2013).

In forestry, the penetration properties of the radar image are of significance to model forest AGB (Kumar *et al.*, 2017). The pulse penetration has a significant influence on the choice of a wavelength and polarisation channel for forest biomass estimation (Lee & Pottier, 2009). The wavelength bands from X, C, S, L, P and polarisation channels of the radar system determines the penetration ability of the electromagnetic pulses and scattering mechanisms of signals received by the radar sensor (Hertz, 2008). Wavelength bands, L and P together with cross polarisation VH and HV are known for their penetration characteristics within the forest layer which in turn results in three types of radar pulse scattering mechanisms (Neumann *et al.*, 2012). The mechanisms are surface scattering or single bounce, double bounce or ground and tree trunk, and volume scattering (Sai *et al.*, 2015). The volume scattering from forest canopy is of importance for forest AGB estimation. Figure 2 shows an example of the volume scattering of L-band cross polarisation as adapted from (Carver, 1988).

A study by (Ghasemi *et al.*, 2011; Mermoz, 2014) confirmed the existence of a strong and positive correlation between AGB/carbon stock and the cross-polarised radar backscatter (HV or VH) of wavelength L- and P-band. However, P band can only be obtained from airborne SAR acquisitions system. The like-polarised radar backscatter (HH or VV) from the shorter wavelength band (X and C) have a weak correlation with AGB/carbon stock (Dobson *et al.*, 1992; Le Toan *et al.*, 1992).

To derive the relationship of SAR and AGB, several techniques have been studied. According to Ghasemi *et al.*, (2011), the estimation of Above ground biomass using SAR is categorised into two main techniques; First using the SAR backscatter values, second using interferometry technique. However, these techniques suffer drawbacks of the saturation problem (Mermoz *et al.*, 2014). For this reason, researchers have pushed toward

the development of SAR processing technique or algorithm known as SAR tomography to solve the saturation problem (Chehade *et al.*, 2016; Ho Tong Minh *et al.*, 2015). This technique uses multiple SAR images acquired at different times to retrieve valuable information for AGB estimation (Ho Tong Minh *et al.*, 2014).

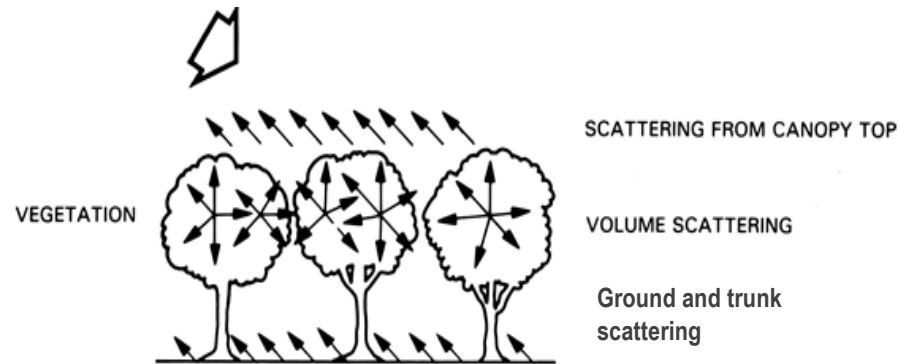


Figure 2: Scattering contribution from the forest (Images adapted from Carver, 1988).

2.2. SAR interferometry

SAR interferometry is a remote sensing technique of using complex images to extract information from SAR images acquired in single-pass or multi-pass (Hurtado, 2012). First SAR interferometry demonstration was done by Graham (1974), where interferometric fringes were obtained by adding signals received from two airborne SAR antennas for topographical mapping. The most potential application of SAR interferometry is the generation of the digital elevation model (DEM), forestry mapping, landslides, hydrology and natural scattering physical parameter extraction (Shane & Papathanassiou, 1998; Lazecký *et al.*, 2015; Zhou *et al.*, 2009).

Single pass: Describes a phenomenon when two antennas on the platform (satellite or aircraft) are used to acquire simultaneously two images of the same area (Shane & Papathanassiou, 1998) (Figure 3a).

Multi-pass: Describes a phenomenon when one antenna on the platform (satellite or aircraft) is used to acquire images of the same area at different time interval also known as repeat-pass interferometry (Shane & Papathanassiou, 1998) (Figure 3b).

Achieving better-quality interferometry results several factors need to be taken into accounts such as the sensor parameters, data quality processing procedure and flight track estimation accuracy. Apart from that, the spatial (baseline) and a temporal decorrelation between the interferometric SAR images affects the interferometric phase estimation. The effects are by introducing noise due to the speckle pattern random change and phase randomisation due to change in backscatter behaviour between interferometric images (Shane & Papathanassiou, 1998).

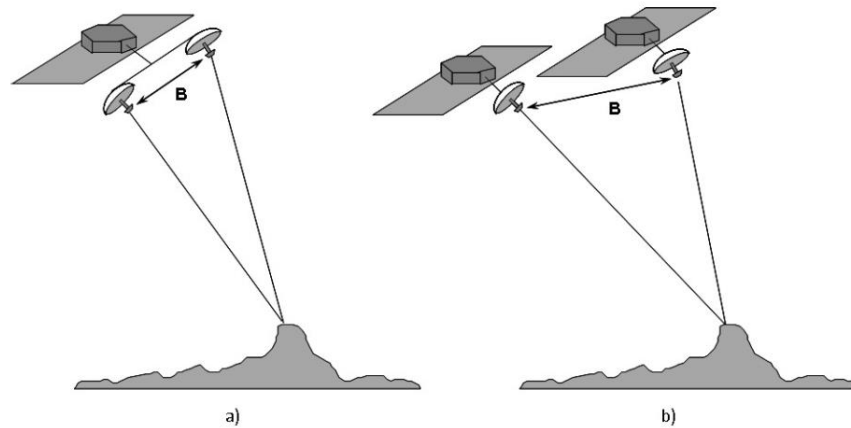


Figure 3: Interferometric imaging geometry. a) Single-pass. b) Multi-pass. Images adapted from Elachi et al., 2006.

2.3. SAR tomography

SAR tomography is an advanced image signal processing technique to generate sections of an image for 3D representation. It is an extension of multi-baseline interferometry concept (Joshi *et al.*, 2017). It utilises the baseline(b), magnitude and phase information to separate out scattered SAR data parameters to retrieve the vertical layers of SAR data at different height levels (Lombardini *et al.*, 2014) (Figure 3). The earlier application of tomography wherein the field of medical imaging such as computed aided X-ray tomography (CT scans), 3D ultrasound, Magnetic resonance imaging, positron emission tomography (Hounsfield, 1979). Also, it has been highly used in determining ice volume and 3D urban building structures reconstruction (Lombardini *et al.*, 2014). Whereas in forestry the first SAR tomography experimental demonstration was done using acquired multi-baseline L- band airborne images to generate tomograms for different polarisations channels (Reigber *et al.*, 2000).

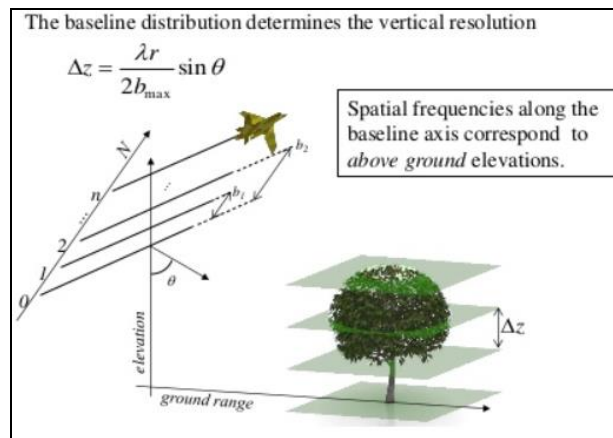


Figure 4: 3D imaging of the forest structure. Δz is a vertical resolution. λ is a carrier wavelength. θ is a radar look angle. b_{\max} the overall normal baseline span (After Hong Tong Ming *et al.*, 2014).

In most publications' SAR tomography is regarded to be a spectral estimation technique (Joshi *et al.*, 2017; Lombardini *et al.*, 2013; Lombardini *et al.*, 2014; Zhu *et al.*, 2010). Various spectral techniques such as Fourier transform to super-resolution techniques have been used to estimate forest biophysical parameters, such as forest height, and AGB (Lombardini *et al.*, 2014).The procedure involved the conversion of multi-baseline

SAR data into multi-layer data, where each layer image represents a complex scene reflectivity of backscatter power at a particular forest height for each resolution cell, Figure 4 is showing an example of multi-layers SAR images.

A study by Ho Tong Minh *et al.*, (2014) investigated the use of SAR tomography for tropical forest biomass estimation using Fourier transform technique. The backscatter power vertical distribution at each slant range and azimuth location were investigated, and the relationship between AGB and backscatter power intensity were established at an interval of 5 meters for different nine forest height layers, ranging from 0 meters to 40 meters height layers. The study found out that, out of nine layers, 30 meters forest layer had the best correlation with AGB and high backscatter power (Figure 5). AGB estimation increased from 250tons/ha to 450tons/ha.

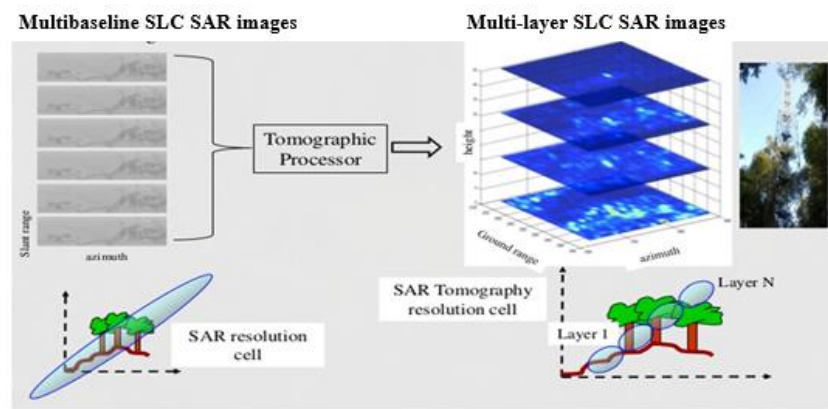


Figure 5: Generation of multilayer SAR images from multi baseline SAR images (After Tebaldini *et al.*, 2011).

2.4. Laser scanners (LiDAR)

In this subchapter, we introduce the two types of LiDAR; namely the Airborne laser scanner and the Terrestrial laser scanner (Figure 6).

2.4.1. Airborne laser scanner (ALS)

ALS is an active remote sensing technology used for deriving digital surface models (DSMs) and digital terrain models (DTMs) of the land surfaces (Sterenczak *et al.*, 2013). The DSMs and DTMs are essential in the extraction of the vertical information of the land features, in this case, the height of forest or commonly known as the canopy height models (CHM). From the CHM, it is possible to extract height of individual trees in the forest. The height is an important parameter for AGB estimation using the allometric equations (FFPRI, 2012; Zawawi *et al.*, 2015). Tree height derived from ALS CHM has proved to be the most accurate of all other methods for AGB/carbon stock estimation (van Leeuwen & Nieuwenhuis, 2010). For example, estimation of tree height from TLS is faced with the problem of occlusion due to several canopy layers in the forest (upper canopy and lower canopy) (Paris *et al.*, 2015). Thus, some studies have suggested the use of TLS to extract DBH and tree height of lower canopies and ALS for extraction of tree height of upper canopies and combine these parameters for AGB estimation (FFPRI, 2012; Paris *et al.*, 2015). The main components controlling the ALS system acquisitions are the Global Positioning System, the laser scanner, and the Inertial Measurement Unit (IMU) (Hyypä *et al.*, 2008).

2.4.2. Terrestrial laser scanner (TLS)

The terrestrial laser scanner is an instrument that uses laser beams to observe and measure the surrounding environment by utilising the angular and range measurements of the reflected beams to derive the 3D point clouds of the objects being observed (Liang *et al.*, 2016). Millions to billions of 3D points are sent to the surroundings and the returned signal recorded by TLS (Kaasalainen *et al.*, 2014) (Figure 6). TLS has gained popularity in its use for estimation of forest biophysical parameters such as DBH, tree height of lower canopies and eventually AGB (Strahler *et al.*, 2008). A result of increasing motivation of replacing conventional method of measuring tree parameter with automatic methods (Liang *et al.*, 2016; Rahman *et al.*, 2017; Seidel., 2012). Recent research results have shown that forest attribute data collected by TLS has high quality and quantity, and the measurements are made to a millimetre level detail (Kaasalainen *et al.*, 2014; Liang *et al.*, 2016). Forest attributes from TLS can also be utilised for different research purposes, such as forest ecology in the estimation of canopy radiation, gap fraction, crown structure, leaf area distributions and leaf area index (Hosoi *et al.*, 2013; Bélanda *et al.*, 2011; Strahler *et al.*, 2008).

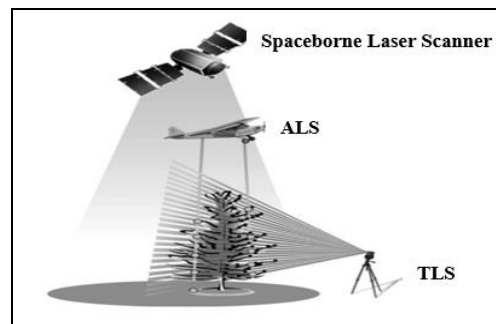


Figure 6: Acquisition geometry of LiDAR remote sensing. (After van Leeuwen & Nieuwenhuis, 2010)

3. STUDY AREA, MATERIALS, AND METHODS

3.1. Study area

This subsection consists of a description of location Berkelah tropical rain forest, vegetation type, topography, and its climate.

3.1.1. Geographical location

The study area is the tropical rain forest of Berkelah, located in Kuantan district-Pahang state, Northeast of Peninsular Malaysia, and is located between 2°57' 43" N and 1001°41' 47" E (Husin & Rajpar, 2015). The District of Kuantan approximately covers an area of 306313ha. The tropical rain forest was chosen because of its vast area coverage and potential in sequestering carbon necessary for climate change measures. Moreover, University Technology Mara Malaysia supported us with the ALS data. They also offered and helped us in executing the fieldwork in Barkelah Forest. The distance from the capital city of Malaysia, Kuala Lumpur to Berkelah is about 255km east of Kuala Lumpur. Figure 7 shows the location map of the study area.

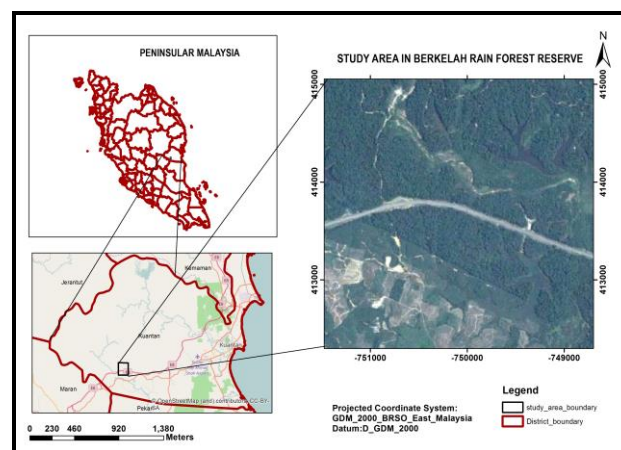


Figure 7: Map of the study area of Berkelah Rain Forest in Kuantan District, Malaysia.

3.1.2. Vegetation type and topography

Low, flat, hilly mountains characterise Berkelah topography, with an elevation of 100 – 120m. The main vegetation type in the study area is tropical rain forests. It is considered to have high species diversity but mainly dominated by species of *Dipterocarpaceae* family (Omar *et al.*, 2015). The tropical rainforest had a mixture of unlogged over primary forest and logged over forest (Rajpar *et al.*, 2014).

3.1.3. Climate

The Berkelah tropical rainforest is situated in the equator area. The climate features are high humidity, uniform temperature, and heavy rainfall with average annual precipitation around 2900mm. There are four different seasons, namely south-west monsoon, northeast monsoon and two shorter periods monsoon-influenced by periodic changes in the wind patterns (Malaysian Meteorological Department, 2017). Berkelah

mean-monthly temperature range from 24.2 °C to 29.9 °C while the average monthly rainfall ranges from 90 mm to 300 mm, with humidity 70% to 98%.

3.2. Materials

A list of materials used for this study was discussed in this section; it includes field equipments and software for data analysis.

3.2.1. Field equipment's and data

Table 1 listed the equipment's used for data collection and datasets used for AGB/Carbon estimation.

Table 1: List of field equipment's, data and their purpose

Field materials	Purpose
TLS Riegl-VZ 400	Terrestrial laser scanner
Garmin GPS	Navigation in forest and sample points location recording
Airborne Laser Scanner Data	Retrieving canopy height model and eventually tree heights
TLS cloud point data	DBH and height measurement for AGB generation and validation
Measuring tape	To outline the circular plot
Field sheets and pencil	Data recording
ALOS-2 PALSAR-2 SAR dataset for September 2016, January 2017 and September 2017	Deriving intensity backscatters, Carbon sequestration estimation, backscatter tomographic layers and produce AGB/Carbon map

3.2.2. Software

Table 2 shows the list of tools and software used for processing and analysis of data used for this study.

Table 2: List of software's and their purpose

Software	Purpose
Snap Toolbox	Co-registration of SAR data Phase calibration of SAR data Interferogram generation Conversion of DN values to SAR backscatter
MATLAB	SAR Tomographic layer generation
ArcGIS- ArcMap 10.3	Producing AGB/carbon map, Tree peak identification
RiSCAN	TLS point cloud processing and analysis
PolsarPro	Interferometry and tomography processing
R -studio	Statistical analysis
LAS Tools package in ArcGIS	DSM, DTM and CHM generation
E-cognition software	Tree crown segmentation
Microsoft office excel	Statistical analysis
Microsoft office word	Project report writing

3.3. Research methods

The research method is an important step to answer the objectives and research questions of this research. It includes fieldwork design, spatial data analysis, statistical data analysis and lastly generation of AGB and carbon stock map. Figure 8 is the flowchart showing the method for the main steps of this research.

Step 1: Biometric data (DBH) preparation and analysis, to be included in the in the allometric equation for above-ground biomass estimation. This step involved the use of ALS to estimate biomass of the upper canopy, through an allometric equation that used the field Diameter at Breast height (DBH) and ALS height.

Step 2: The processing of point cloud data from the Terrestrial Laser Scanner, which involved point cloud registration and filtering, and later the individual tree extraction. From each tree, the lower canopy tree height was measured and later combined with the associated DBH from step 1 into the allometric equation for AGB estimation.

Step 3: The ALS data was processed to retrieve digital surface model (DSM) and digital terrain model (DTM). Followed by subtracting DTM from DSM to get the CHM used for upper canopy tree height extraction by overlaying it with tree point locations. The resulting tree height was combined with associated DBH from step 1 into the allometric equation to estimate AGB.

Step 4: This step involved calibration of the SAR images to backscatter coefficient, Image geo-referencing and filtering of the backscattered images to be used for AGB model development, AGB Estimation, validation and carbon estimation.

Step 5: Tomographic analysis of the SAR data to retrieve the vertical distribution of backscatters was done. This step also included interferometric wave number generation in order to derive the height. Followed by interferometric analysis to retrieve canopy height model of the study area (CHM). Then a comparison between SAR derived CHM, and LiDAR CHM was made.

Step 6: Involved developing regression models between single and time series SAR image backscatters and Field AGB. Followed by model validation to derive the model accuracy in AGB estimation. The estimation accuracy was determined based on the coefficient of determination, the root mean square and p-value results. Amount of carbon sequestered in september 2016/2017 was also determined at this step. Also, multiple regression of HV, HH and AGB was done to determine if there is a significant improvement in AGB estimation in relation to a lone HV regression model.

Step 7: This step involved determining the saturation point of AGB in relation to backscatter.

Step 8: This step involved mapping of AGB and carbon based on the best model from step 6.

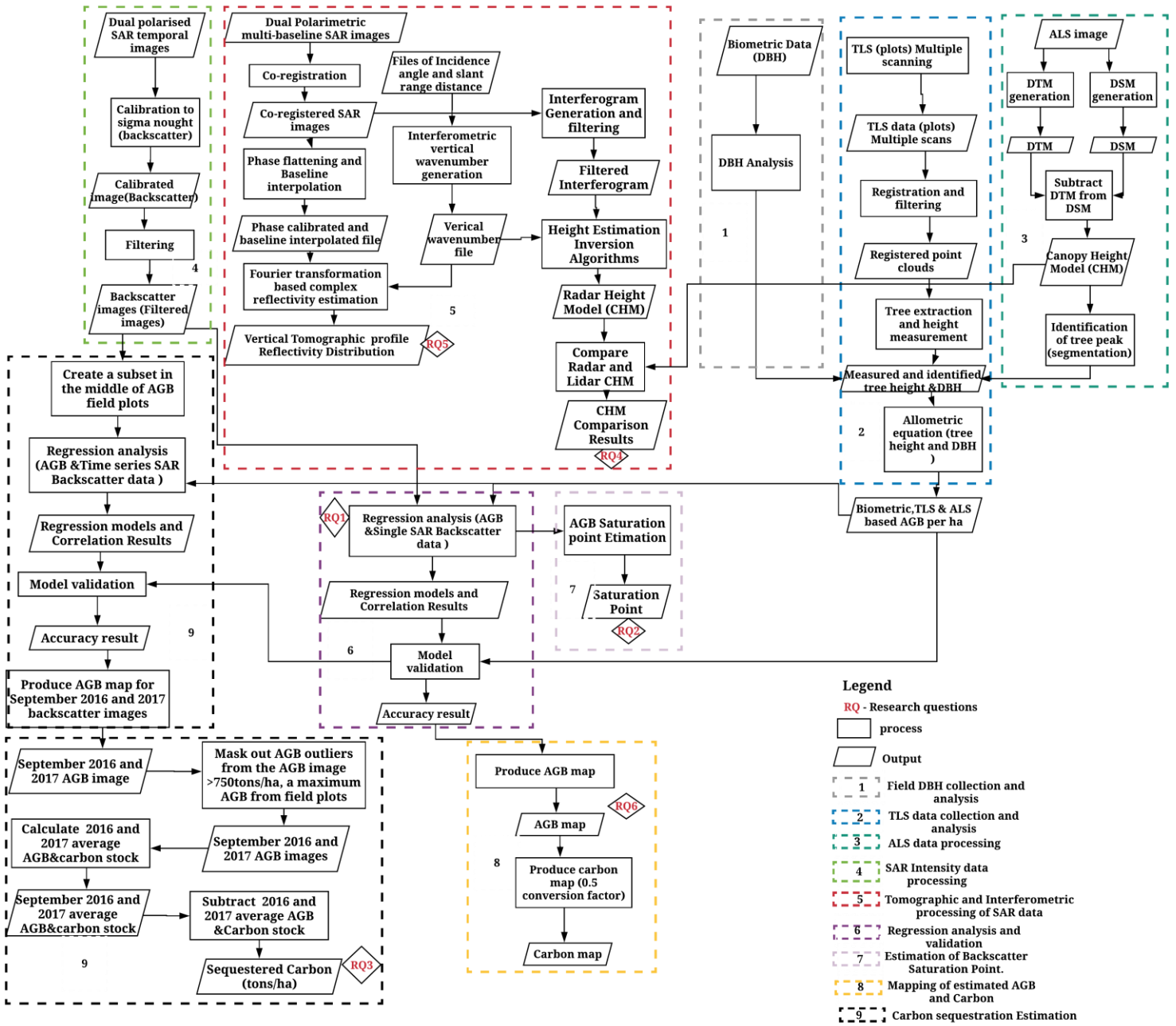


Figure 8: Flowchart of the research method

3.4. Field work

3.4.1. Field sampling design

The purposive sampling design was employed in establishing sample plots for data collection. The design is based on the judgement of the researcher. The choice of which was based on the accessibility to sample plots,

time-saving and slope of the area. Purposive sampling has an advantage over other sampling design based on its ease of implementation and accessibility of samples over the entire study area. About 38 sample plots were collected based on the criteria as described in the following:

Accessibility: Areas with fewer obstacles like water streams, less undergrowth was considered since it was easy to move from one plot to another hence collecting more sample plots per day.

Time: To be able to collect the desired number of samples, purposive sampling was the best option, since it makes it easy to move from one plot to another.

Slope: Less steep areas were favoured because TLS is a heavy (27kg) and delicate equipment to carry on a steep slope. So, to save time and avoid damage to the TLS less sloppy areas were preferred over high sloppy areas.

3.4.2. Determining plot size

The objective and purpose of the research are the most determining factors of the shape and size of plots to be used for data collection (Tree DBH and Height). Plots shape varies from circular, rectangle and square. Circular plots are the most suitable, preferred and used plot shape for forests above ground biomass assessment and forest inventories (Laar *et al.*, 2007). Circular plots have the advantage of ease plot establishment and less number of borderline trees; other plot shapes produce a greater number of border trees in a plot, which induces systematic error in plot sampling (Kershaw *et al.*, 2016; Laar *et al.*, 2007).

According to Luo *et al.*, (2017), biomass estimation is affected by choice of plot size. The optimal plot size for biomass estimation varies for different study areas and vegetation types (Estornell, 2011). Therefore, it is essential to determine an optimal plot size which will not significantly affect the accuracy of biomass estimation before going for data collection.

A study by Gobakken *et al.*, (2008) showed that a plot size of 0.05ha or 500 square meters is sufficient to give an accurate result for biomass estimation, as increasing the plot size beyond 0.05ha - 0.06ha would not significantly improve the results for biomass estimation. They also revealed that plot size beyond 0.1ha is hard to demarcate and increases need for slope correction to be done for many plots. In this study, a circular plot of 0.05ha (500m²) equivalent to the radius of 12.62 as used by (Gobakken *et al.*, 2008) was adopted. The plot size between 500-600m² significantly increase the number of trees to be measured in each plot. Therefore, it is a cost-effective plot size (Ruiz *et al.*, 2014).

3.5. Data collection

The field data was collected from 23rd September to 11th October 2017. From each established plot the tree DBH and height were collected. The Alos-2-Palsar-2 data were acquired from JAXA on 1st November 2017. The following steps describe the process carried out during thesis data collection.

3.5.1. Biometric data collection

The circular plot of radius 12.62m was established using a tape measure after the sample plot was purposively selected. Tree DBH at a 1.3m height above the ground was measured using the diameter tape in each plot. Only trees with DBH more than 10cm was measured since they have a significant contribution to aboveground biomass (Brown, 2002). The coordinates of each tree in a plot were recorded using a tablet GPS.

This was important for identifying each measured tree located in a plot for height extraction from the canopy height model. The field data sheet was used for recording the tree DBH and coordinates respectively.

3.5.2. Data collection with TLS

After establishing a circular plot of radius 12.62m as in subsection 3.5.1. Trees with DBH ≥ 10 cm were labelled with numbers on laminated papers facing plot centre direction; Trees with DBH < 10 cm were not considered as they have low contribution to AGB estimation (Brown, 2002). Labels are essential to ensure trees are identified on the TLS scan and related to trees on the ALS-CHM. After labelling, the retro-reflectors were placed in near and outer scan position of plots; these were used as tie points for registration and georeferencing. Using RIEGL VZ-400 TLS, multiple scanning of four positions was done in a plot to record all sides of the tree or obtain a 3D representation of trees (Srinivasan *et al.*, 2015). Multiple scan scenario as in Figure 9.

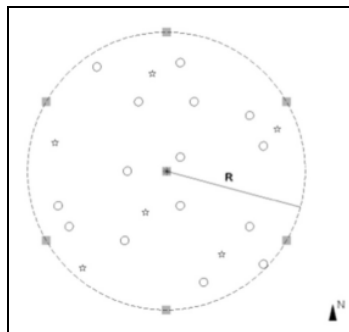


Figure 9: Multiple scans. Circular plot with radius R. Plot centre marked using an asterisk. The scanning position indicated by squares. Tree positions in solid circles. Trees with retro-reflectors shown using stars (As adapted from Liang *et al.*, 2016).

3.5.3. ALS data acquisition

The Berkelah tropical rain forest, Malaysia airborne laser scanner data were acquired on 12/11/2014 by the Airborne Research and Survey Facility and obtained for this study from the University of Technology Mara Malaysia. The data were supplied in ASCII and LAS 1.2-point clouds files format, and they were classified into two classes as class 1 and class 7, the later was classified as noisy points. The point clouds data contained a total of four returns between 1 and 4 were the 1 is the first return, and 4 is the last return. The data were supplied in horizontal datum: WGS84, vertical datum: WGS84 and projection: UTM48.

3.5.4. Alos-2-Palsar-2 SAR data acquisition

The ALOS-2 is the Japan Aerospace Exploration Agency Advanced Land Observation Satellite 2 which carries on board the Phase Array L-band Synthetic Aperture Radar 2 (PALSAR-2) Sensor. Three Dual polarised ALOS-2 PALSAR-2 images used for this study. The images were acquired from JAXA through the Remote Sensing Technology Center of Japan (RESTEC) which is responsible for distribution of remote sensing data obtained from JAXA (Restec, 2000). The date of scenes observation was 9/09/2017, 28/01/2017 and 10/09/2016. The images were acquired from Restec by Faculty of Geoinformation science - University of Twente on two-time period, on 01/11/2017 for the first two images and 28/09/2017 for the third image respectively.

3.6. Data processing and analysis

3.6.1. Terrestrial laser scanner data processing

Point cloud registration and plot extraction

RiSCAN PRO software was used for Registration of plots multiple scans, using automatic marker-based registration which uses tie points to merge multiple scans precisely. This is essential for correct point cloud Geo-referencing. The automatic marker -based registration method is less time-consuming. Thus it is more preferred over the course manual point cloud registration method.

After registration, the plot extraction was done to remove trees which are outside of the circular plot. The extraction was done using the range function in RiSCAN PRO. Only trees within the established circular plot were extracted from the registered point clouds.

Individual tree extraction and tree height measurement

The individual trees extraction, Measurement of Tree parameter (Tree height for lower canopy trees) was done using the RiSCAN PRO software. This was done by using the A selection mode tool was used and later saved as polydata. The tree tag number was used as the basis for naming the polydata. The latter step was to measure the tree height of lower canopies by measuring the distance between the trees lowest and highest point cloud in RiSCAN PRO. The tree height value was recorded to be combined with respective DBH in the allometric equation for AGB estimation.

3.6.2. Airborne laser scanner data processing

In addition to field data, tree height measurements were extracted from Airborne LiDAR canopy height model data of the study area. The extraction of tree height from the LiDAR point cloud data was done using Las tools package. To get the canopy height model, first the point clouds data were classified into the ground and first return point clouds. The first return point clouds were used for DSM creation, and the last return(fourth) were for DTM creation (Figure 10a, b). Then the canopy height model (CHM) was simply obtained by subtracting DTM from DSM (Figure 10b). The CHM was created with 1m pixel size to reduce uncertainties associated with identifying the treetop during tree height extraction. To extract tree height, Tree canopy segmentation was done in e-cognition software to generate a vector layer (shapefile) with segmented polygons. The Multiresolution segmentation process was done by setting the best parameters based on trial and error approach (compactness 5, shape 9). Later the CHM was overlaid with the segmented shapefile, to extract the maximum value for the pixels falling within the segments of the segmented vector layer. Then the pixels were assigned a new maximum value to be taken as a treetop height (Figure 10c). The process was done using Zonal statistics tool (spatial analyst toolbox) and extract multipoint data in ArcGIS.

To extract tree height the shapefile from segmentation was overlaid on the CHM, together with the plot centres location, shapefile of field circular plot and the individual tree location. From the overlay, the maximum elevation was used to identify the height of each tree in a plot. Lastly, the derived tree height from ALS and TLS was combined with Biometric DBH information in an allometric equation 10 to estimate AGB for each tree.

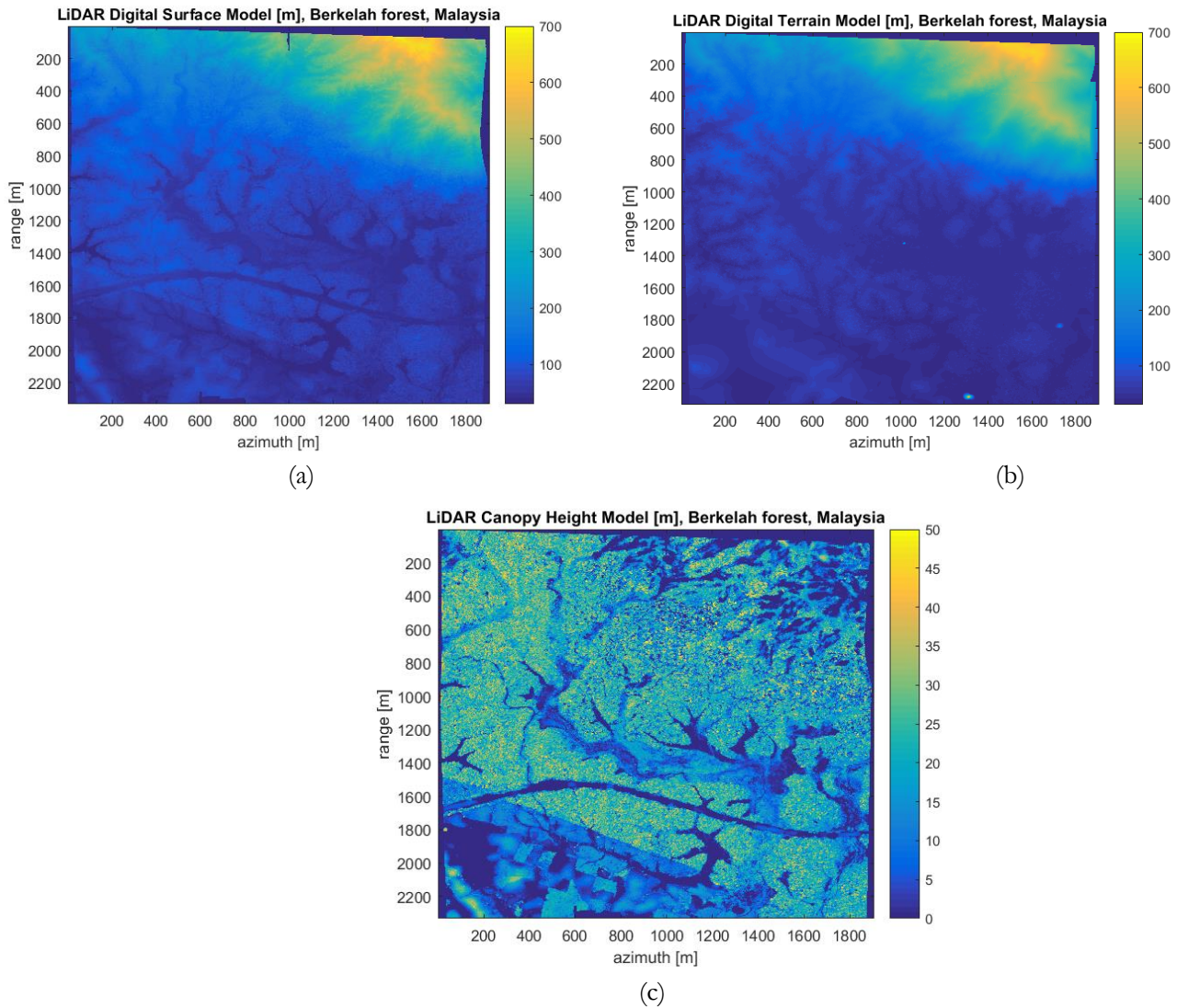


Figure 10: LiDAR digital surface model (a), Digital terrain model (a) and Canopy Height model (c) of the study area.

Although measurements from LiDAR data are considered to be of high accuracy and precise compared to satellite data sources, it is essential to note that the LiDAR data are highly expensive, and they are limited to be made in stormy, wind and cloud cover areas.

3.6.3. ALOS-2 PALSAR-2 SAR data pre-processing for backscatter retrieval

SAR image pre-processing is an important step in image analysis for AGB estimation. The SAR image where obtained at level 1.1 as a complex image, for which most of the pre-Processing step such as radiometric calibration and geometric correction has not been done. Pre-processing of SAR images aims to correct for degradation and distortion in the image and represent a meaningful information of the scene image. For level 1.1 complex images, the first step was a geometric correction and Geo-referencing, followed by retrieval of SAR backscatter from the complex images and Filtering was applied in Snap software.

Geometric correction and geo-referencing

The single look complex SAR images are geometrically distorted due to the sensors image acquisition not being at Nadir location, tilting of the satellite sensor and image scene topographical variation (Schreier,1993; Small *et al.*, 2008) (Figure 11). Thus, geometric correction is aiming to compensate these distortions so as the SAR images can represent the real world.

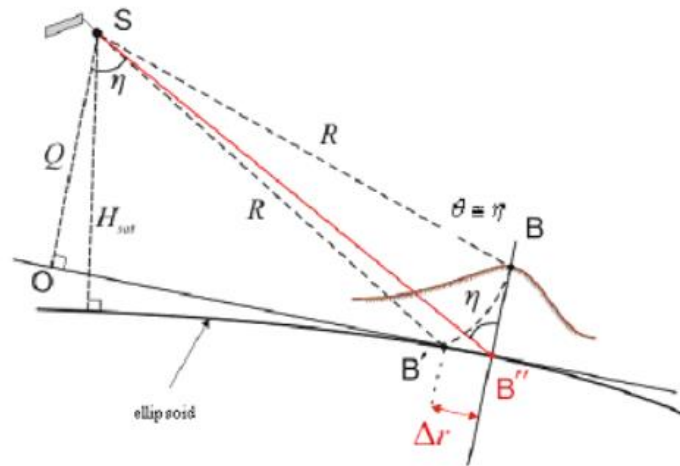


Figure 11: The SAR image acquisition geometry of topographical distortions. Point **B** through elevation **h** directly above the ellipsoid is imaged at position **B'** in SAR image. However, its real position is **B''**. The **B'** and **B''** offset Δr , displays the topographic distortions effect on SAR image (Schreier, 1993).

Subsequently, in order to have a true projection, the SAR images were re-projected to Universal Transverse Mercator (UTM) coordinate system, zone 48N as the coordinate system used for the study area (WGS_1984_UTM_Zone_47N).

In the meantime, the georeferenced and re-projected SAR image were opened in ArcGIS, then overlaid with the boundary shapefile and then the image was clipped using the study area boundary shapefile.

3.6.4. Retrieval of radar backscatter coefficient and radiometric correction

The retrieval of radar backscatter coefficient was done to both cross and like polarised images. First, by applying calibration to radar images; this was done by considering the image processing level, pixel size and the field sample plot size. Calibration was done in SNAP software using band math; the DN values were converted to the backscatter coefficient for ALOS PALSAR images level 1.1 by use of equation (1) as proposed by (Shimada *et al.*, 2009).

SAR data have a characteristic of salt and pepper like appearance (Radiometric distortion). The salt and pepper appearance or speckle noise which can have an influence on the relationship between the imaged object and the received backscatter interactions (Joshi *et al.*, 2015). Thus, it is important to apply Speckle filtering to smooth the image or correct for this distortion. For this work, Lee speckle filter was applied on all the retrieved backscatter cross polarized SAR images. The output filtered image would have much smooth texture and reduced variance. Figure 12 is one of the Original SAR image (a) as compared to the filtered SAR backscatter image (b).

Equation 1: Equation for retrieval of backscatter coefficient

$$\sigma^{\circ} 1.1 \text{ product} = 10 \cdot \log_{10}(I^2 + Q^2) + CF - A$$

Where: $\sigma^{\circ} 1.1 \text{ product}$ = Normalized Radar Cross Section of level 1.1 product in (dB)

I = Real part of SAR image level 1.1 SLC product

Q = Imaginary part of SAR image level 1.1 SLC product

CF = Calibration Factor of -83.0dB

A = Constant 32.0

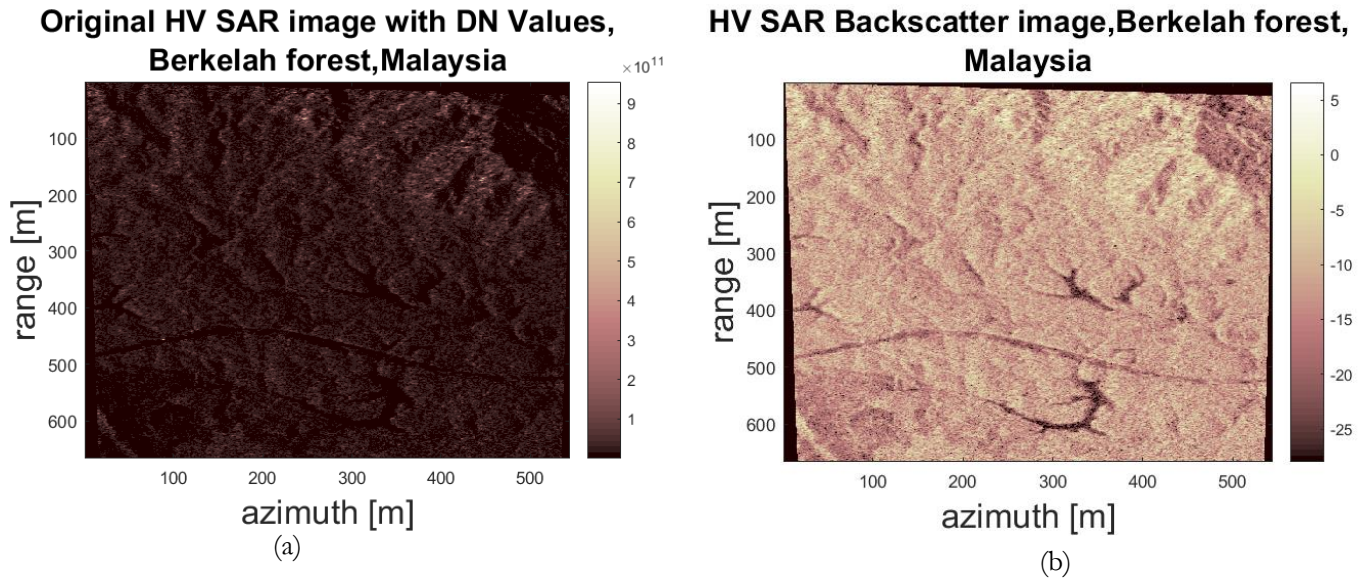


Figure 12: Raw SAR image as compared to backscatter image. HV images with DN values (a) and δ° (b). Objects in a backscatter image are more clearly visible than the original image with DN values which appears dark.

After converting the DN values to backscatter coefficient, the backscatter coefficient was retrieved as; the plot centre point location was overlaid on the backscatter coefficient image and the average of backscatter for 5 by 5 pixels covering the field plot was extracted as in Figure 13. The 5 by 5-pixel window was chosen so that the whole plot area (diameter 25.24m) and an additional 5m GPS error is included in calculation of plot AGB. This approach tends to smoothen out the average backscatter, but in so doing it reduces the error of excluding backscatter signals from trees within the plot (Sumareke, 2016). The extracted backscatter were used for AGB model development and validation.

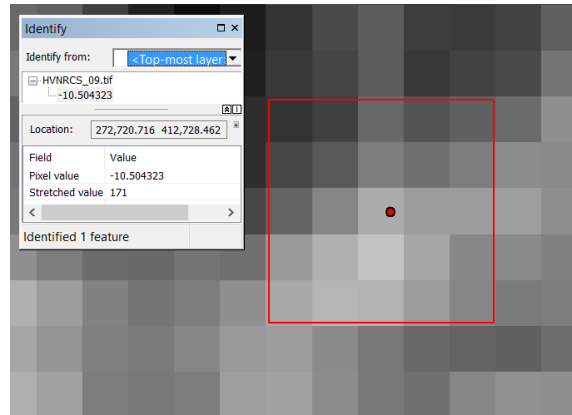


Figure 13: Backscatter retrieval from cross-polarized backscatter coefficient SAR image.

3.6.5. Above-ground biomass saturation point estimation

AGB Saturation point can be defined as a point when the slope of the curve of the logarithmic regression starts to decrease by 0.02dB against the minimum-maximum of the AGB (Suzuki *et al.*, 2013). From the regression analysis of the Above-ground biomass and L-band cross-polarized radar backscatter, The AGB saturation point was calculated along the logarithmic regression line by estimating the point where the slope started to decrease by 0.02dB using slope equation 2.

Equation 2: Equation for determining the AGB saturation point

$$\text{Slope} = \Delta Y / \Delta X \quad (\text{Suzuki } et al., 2013)$$

Where: ΔY is the change in backscatter values with respect to the minimum value

ΔX is the change in AGB with respect to the minimum AGB value

3.6.6. Retrieval of radar backscatter coefficients for time series analysis of AGB/carbon stock and carbon sequestration

On the assessment of the time-series of AGB/carbon sequestration, a subset of 50ha from the study area backscatter images was extracted in the middle of the fieldwork forest AGB/carbon stock plots as in Figure 14. Then Areas with backscatter outliers (Backscatters from open areas, reflectance object, roads) were masked out. The outliers were masked out using the highest AGB value 750ton ha⁻¹ from the field as a cut-off value point; the reason was to remove the effect of outliers on AGB/carbon stock over-estimation and eventually on carbon sequestration. These outliers showed up because of high slope areas facing the radar antenna, corner reflectors, etc. Three steps were used to assess the relationship between AGB and time series of L-band polarised Radar data (Table 3). The first step was taking the plot backscatter values of the 10/09/2016 cross-polarised image and derive a linear relationship with AGB. Secondly taking the plot backscatter values of the 09/09/2017 cross-polarised image and derive the relationship with AGB. The third step, the developed models were used to estimate the AGB/carbon stock of the two-year images, first by applying the first step model to both images, secondly by applying the models independently. The sequestration was estimated based on the difference of the average AGB/carbon Stock between the two-year images. Here, the logarithmic regression models were used because of having high R² and low RMSE.

Table 3: SAR parameters and Models used for time-series Analysis for AGB/Carbon Stock Sequestration.

Steps	Parameters, Models
1	HV(dB)-Sep 2016, AGB
2	HV(dB)-Sep 2017, AGB
3	Model-1 (HV(dB) = 1.7542ln(AGB) – 22.031), Model -2 (HV(dB) = 1.728ln(AGB) – 21.967)

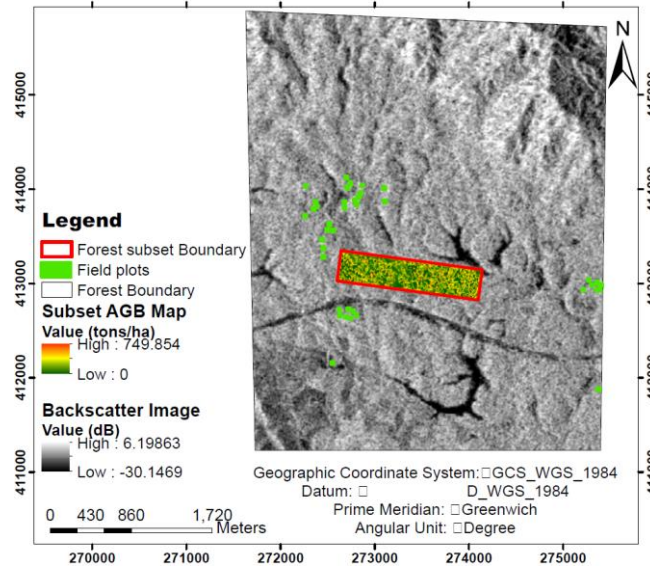


Figure 14: The map of subset area used for estimation of carbon sequestration between the year September 2016 and September 2017.

3.6.7. Multiple logarithmic regression analysis of AGB and L-band HV, HH polarised radar backscatter in relation to single HV backscatter

Apart from using only the cross polarised backscatter to estimate AGB/carbon stock. We also decided to investigate if there is a significant improvement on AGB estimation if the like polarised backscatter (HH) is added to multiple regression analysis. In this case, a multiple regression model of HV and HH backscatters as dependent variables and AGB as an independent variable (Equation 3). On using multiple logarithmic regression, a relationship between HV, HH backscatter values and AGB was derived, a comparison on results of multiple logarithmic model and single parameter logarithmic model were analysed based on R², Root mean square error (RMSE) and probability value (p-value).

Equation 3: Multiple logarithmic equation AGB and HV, HH polarised backscatter

$$\ln(\text{AGB}) = a * \text{HV} + b * \text{HH} + c$$

Where a, b and c are constants derived from the regression relationship.

3.6.8. ALOS-2 PALSAR-2 SAR interferometry processing

In this section the processing procedure for interferometry height estimation from SAR data is explained. The procedure involves several steps such as Image sub-setting, Co-registration, Interferogram generation and coherence estimation, Interferogram flattening, Vertical wavenumber estimation and Height estimation. The DEM differencing algorithm height estimation methods from interferometric SAR images were utilised.

Image sub-setting

The ALOS-2 PALSAR-2 SAR data covers an area of about 70km x 70km while our study area only covers about 4km x 4km, Processing the whole image would increase processing time and processing areas outside our study area which are of no interest. Therefore, subsetting the images were done importantly to minimise processing time and restrict ourselves to the study area of interest.

Co-registration

After image sub-setting, the two SAR images were correctly aligned by co-registering them to a subpixel accuracy by making sure that the pixels in one image properly matches the pixels in another image. A transitional shift characterises the acquisition geometry of different SAR images acquired in the same mode; this results in improper alignment of the SAR images. Hence the resulting interferogram would have low coherence and imprecise phase difference information. The image co-registration process requires assigning one image as a master and the other as a slave image for which the slave image is transformed to match the master image. Cross-correlation was used to match corresponding points from slave to master image. For this study, the images of 09/09/2017 were assigned as a master image and the image acquired on 28/01/2017 as a slave image. The two steps were followed during the co-registration: The first being course registration and then fine registration.

Generation of an interferogram and complex coherence

Once the co-registration was done, the complex images (real and imaginary part) of the SAR images were used for generating the interferogram. The interferogram is obtained by taking the phase difference between two complex images (master and slave) equation 4, of which the resulting difference ranges between $[-\pi \pi]$. The complex coherence of the phase between two images is obtained as a cross-correlation between the two images obtained by the equation (4), the resulting coherence ranges between 0 and 1.

Equation 4: Equation for Interferogram Generation

$$\Delta\phi = \phi_2 - \phi_1 = \frac{4\pi\Delta R}{\lambda}$$

Where,

$$\phi_1 = \frac{4\pi R}{\lambda}, \quad \phi_2 = \frac{4\pi(R + \Delta R)}{\lambda}$$

Looking at the interferometric coherence images Figure 15 and 16, we see bright and dark spots (areas), the bright areas represent areas of high coherence while the dark areas represent areas of low coherence. The coherence pattern corresponds to the interferogram phases pattern. Fringes can be seen in areas with high coherence, as opposed to areas with low coherence. Each colour phase in the interferograms corresponds to a complete phase difference. The coherence images in forest areas appear dark due to a loss of coherence as a

result of volume scattering, while areas of stable terrain such as open areas and roads appears bright due to high coherence. The HH coherence image appears brighter than the HV coherence image due to characteristics surface scattering of the HH as compared to more volume scattering of signals from HV images.

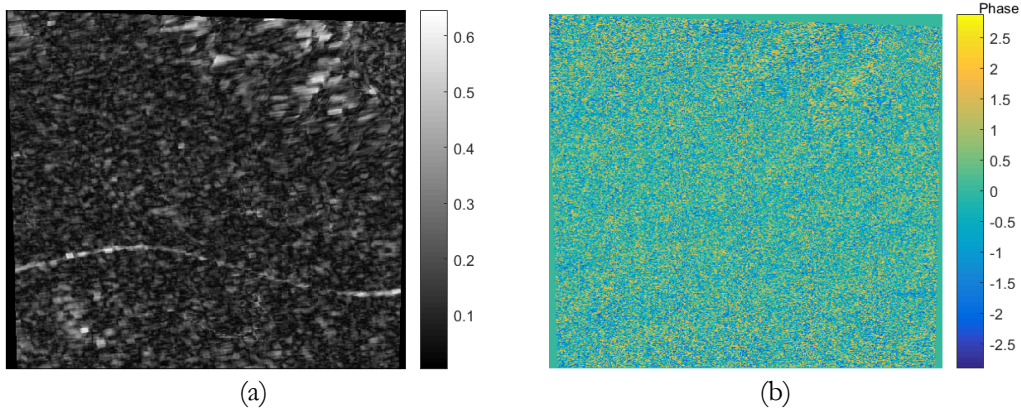


Figure 15: HH Interferometric coherence and phase of the study area. a) HH coherence image. b) HH interferometric phase

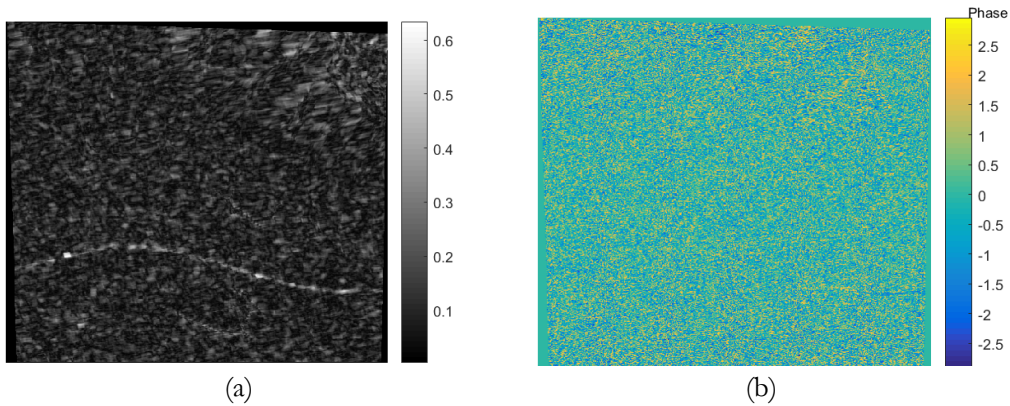


Figure 16: HV Interferometric coherence and phase of the study area. a) HV coherence image. b) HV interferometric phase

Interferogram flattening and filtering

For better quality of the derived interferogram for height estimation, the flat earth phase which corresponds to earth curvature of the earth reference surface was removed. The flattened interferogram phase is estimated using equation (5), the flat earth phase was subtracted from the complex interferogram to obtain the interferogram with phases related to elevation (without flat earth phase). Noise characterises the interferometric phases. To remove the noise, Goldstein speckle filtering were applied to the interferogram to increase the signal to noise ratio, Figure (17).

Equation 5: Equation for generating the flattened interferogram

$$\phi_{FLAT} = -\frac{a2\pi h}{\lambda R \sin(\theta_0)} B \cos(\theta_0 - \alpha) = -\frac{a2\pi B_n h}{\lambda R \sin(\theta_0)}$$

Where B_n , λ , R , h and θ are the perpendicular baseline, wavelength, Slant-range distance, elevation of the scene imaged and incidence angle respectively.

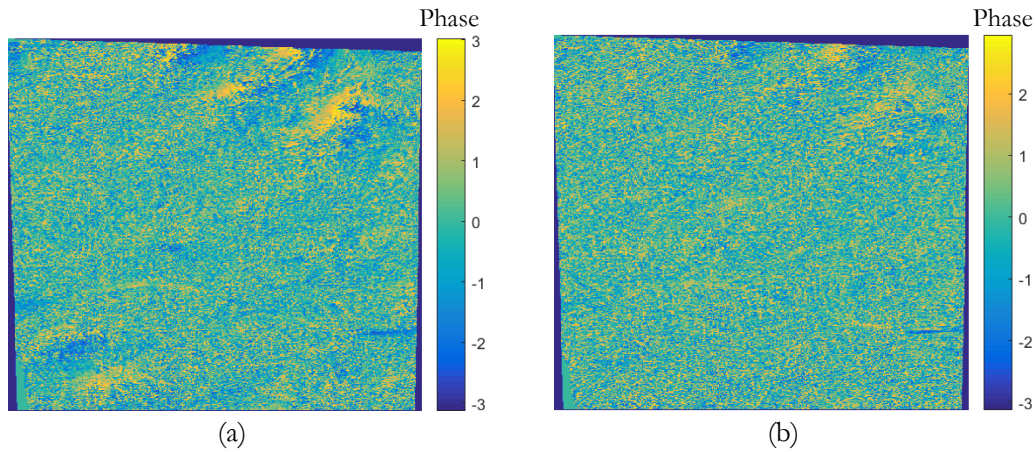


Figure 17: Images of flattened and filtered interferogram for HH and HV polarised SAR images. The phase difference is more pronounced in HH than in HV interferogram. a) HH interferometric phase flat earth removed. b) HV interferometric phase flat earth removed

Generation of the Interferometric vertical wave number

A critical parameter for height estimation from SAR interferometry is the use of vertical wavenumber. Interferogram represents height variation in phase domain with values ranging from $-\pi$ to $+\pi$. So, to change from phase to height encompasses the use of vertical wave number. The vertical wavenumber was calculated using equation (6). Figure 18 shows the interferometric vertical wavenumber of the study area derived from SAR images.

Equation 6: Equation for calculating the vertical wavenumber

$$K_z = \frac{4\pi B_n}{\lambda R \sin(\theta)}$$

Where B_n , λ , R and θ are the perpendicular baseline, wavelength, slant-range distance and incidence angle respectively.

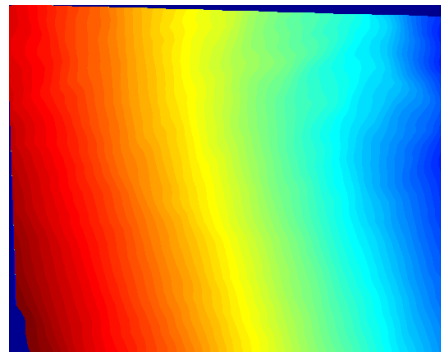


Figure 18: Interferometric vertical wavenumber of the study area derived from SAR images

Generation of forest height (CHM) using forest height inversion algorithm

DEM differencing inversion algorithms were used for height estimation. With DEM differencing approach the height estimate was generated by isolating the polarisation (HH) channel that scatters from the forest canopy top as in equation 7. The HH polarisation was taken due to its characteristics of surface scattering as compared to volume scattering by HV polarisation (Cloude, 2005). Figure 19 shows the Height variations of the study area derived from SAR images using DEM differencing forest height inversion algorithms results.

Equation 7: DEM differencing Algorithm

$$h_v = \frac{\arg(\gamma_{\underline{w}_v}) - \hat{\phi}}{k_z}, \quad k_z = \frac{4\pi\Delta\theta}{\lambda\sin\theta} \approx \frac{4\pi B_n}{\lambda R\sin\theta}$$

Where h_v is the forest height, \underline{w}_v is selected polarisation and k_z is the vertical wavenumber

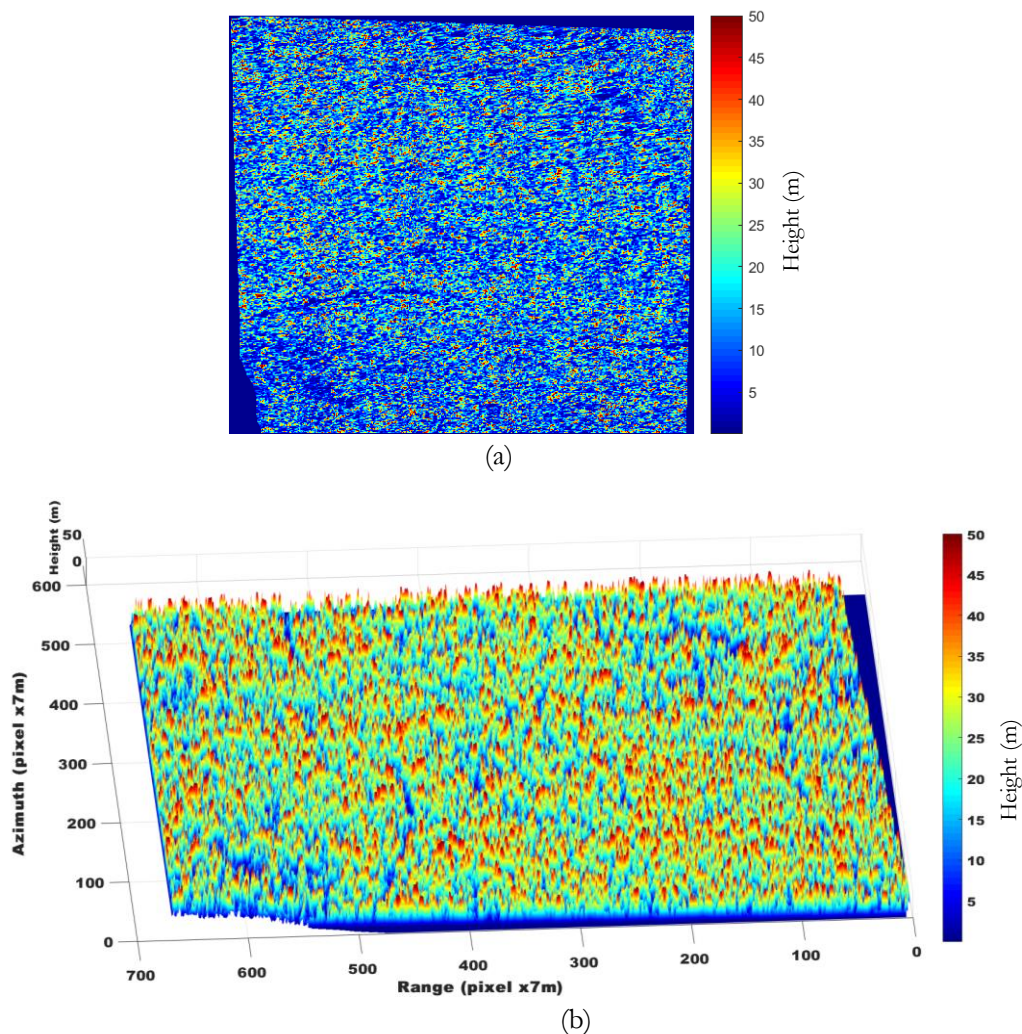


Figure 19: The Height variations of the study area derived from SAR images using DEM differencing forest height inversion algorithms. (a) 2-D CHM Visualization (b) 3-D CHM Visualization

3.6.9. Tomographical retrieval of backscatter distribution

TomoSAR processing provides the 3-D of the SAR data (Ho Tong Minh *et al.*, 2015). From the SAR 3-D data, we can retrieve the distribution of backscatters from the forest canopy layers (Kumar & Kumar, 2017). The tomographic backscatters from radar image can be associated to represents scattering contributions for certain heights of the forest. The reconstruction of the tomographic backscatters in height direction was done by converting the SAR multi baseline interferometry data into the multi-layer data. Which was achieved by taking a Fourier transformation of the multi-baseline data along the baseline direction (equation 8), where at each range and azimuth location there is a complex scene reflectivity.

Equation 8: Fourier transform

$$S(z) = \sum y_n(\mathbf{r}, \mathbf{x}) \exp[-jk_z(\mathbf{n}) \cdot z]$$

Where: $S(z)$ is complex reflectivity along cross range direction for each pixel at a given layer height

$y_n(\mathbf{r}, \mathbf{x})$ is complex valued pixel for SAR image

K_z is the interferometric vertical wavenumber

Z is layer height

Moreover, using equation (9), the backscattered power distribution can be retrieved in a cross range distribution (Kumar & Kumar, 2017). As a result, we retrieve the backscatter vertical profile and the cross-backscatter layers fixed to a certain height of the forest, e.g. 5m layer, 10m layer, 15m layer, 20m layer, etc. (Ho Tong Minh *et al.*, 2014).

Equation 9: Backscattered power distribution

$$P(z) = |S(z)|^2$$

3.6.10. Above-ground biomass calculation

AGB computation was done using the lower canopy tree height from TLS and upper canopy tree height from ALS, combined with field DBH data. For this study, AGB of 23 plots of Berkelah tropical rain forest was estimated using an improved allometric equation 10 for the tropical forest by (Chave *et al.*, 2014).

Equation 10: Allometric Equation

$$AGB_{est} = 0.0673 * (\rho D^2 H)^{0.976}$$

Where: AGB_{est} is above ground biomass estimated in Kilogram

D is diameter at breast height in centimetre

ρ is wood density in gcm^3

H is height in meter

0.0673 and 0.976 are constants

3.7. Statistical analysis

To answer the research objectives and questions the following statistical analysis was done as in the following sub-sections.

3.7.1. The relationship between AGB and L-band cross polarised radar backscatters

The statistical regression analysis was used to assess the relationship between the AGB and retrieved backscatter values from the SAR image. The regression model for AGB based on backscatter intensity values was produced, and AGB was predicted using the resulting regression model.

3.7.2. Estimation of the backscatter saturation point

The calculation of saturation point was done at each point along the graph of the regression line. The saturation point was selected at a point where the slope of the regression line started to change by a factor of 0.02dB.

3.7.3. The relationship of AGB, time series L-band cross polarised radar backscatters and carbon stock sequestration

The time series logarithmic regression analysis was used to assess the temporal influence of SAR backscatter values to AGB estimation and eventually carbon stock estimation; this was done by retrieving the relationship between backscatter from the forest at different periods and the field AGB. The relationship was assessed based on the best results of coefficient of determination and Root mean square error.

3.7.4. The relationship between interferometric height and LiDAR height

The trend of height variation using a straight line drawn on the interferometric and LiDAR height maps, together with the regression analysis from average height values from the field plots was used to assess the relationship and accuracy of ALOS-2 PALSAR-2 L-band SAR data for height estimation against that of LiDAR height.

3.7.5. The tomographic distribution of L-band cross polarised radar backscatters in relation to AGB

The vertical tomographic slice from a stack of L-band SAR images was used to analyse and interpret the distribution of SAR signals coming from the forest, and their effect on AGB estimation was discussed. The slice was compared with the observed physical features of the study area using a study area map.

3.7.6. Above-ground biomass (AGB) and carbon stock estimation and mapping

Using the logarithmic regression model from step 3.6.6, the AGB was mapped for the study area forest and also the amount of carbon stock was estimated and mapped using a conversion factor of 0.5 as given in equation 11 (Hirata *et al.*, 2012). The interpretation of this equation gives half of AGB as the carbon stock stored in a forest. Total AGB for the study area was also calculated by summing up the amount of AGB in all pixel of the image. Areas with water bodies and corner reflectors were masked out in total AGB calculation. Masking out were done using the minimum (8.7tons ha⁻¹) and maximum (750tons ha⁻¹) field AGB.

Equation 11: Carbon Equation

$$C = B * CF$$

Where: C is the carbon stock in tons, B is the dry biomass and CF is the carbon fraction (0.5)

4. RESULTS

4.1. Statistical analysis of field data

Biometric methods and terrestrial laser scanning were used for field data collection. The tree diameter at breast height was collected using only biometric method (diameter tape) while tree height data from trees which were not visible from the airborne laser scanner data were retrieved from TLS data. About 23 plots data collected from the field and a total number of 660 trees were used for the above-ground biomass calculation and statistical analysis. The mean above-ground biomass is 316ton ha⁻¹ and the stand basal area is 35.46 m² ha⁻¹. The descriptive analysis of the forest parameters such as basal area, AGB, DBH, height is given in Table 3.

Table 4: Summary statistics of forest parameters.

Item	Number of plots	Minimum	Maximum	Sum	Mean	Median	Standard Deviation
	Statistic	Statistic	Statistic	Statistic	Statistic	Statistic	Statistic
Trees/plot	23	15	60	1030	32	32	1.6
BA (m ²)	23	0.03	3.53	51.93	1.62	1.67	0.14
AGB (ton)	23	8.7	701	11329.95	316	279.69	33.07
DBH(cm)	23	13	33	697	22	22	0.77
Height (m)	23	5.7	37.56	716.46	22.39	23.02	1.35

Further AGB analysis shows that the AGB is somewhat normally distributed (Figure 20b) with 0.07 skewness value, However, it is also true that more frequency of AGB distribution is observed at higher AGB values. From the AGB histogram and density plot in Figure 20, it can be observed that we have an increase in AGB up to 200 tons ha⁻¹ after which there is a sudden decrease in AGB, then an increase in AGB again is observed from 380tons ha⁻¹. This shows that the vegetation structure of the study area is more variable, in this case we have higher values of AGB (larger trees) with less regeneration of young vegetation. From the density plot (Figure 20a), the peak density of AGB is observed at two peaks at about 0.002 where AGB ≈ 200tons ha⁻¹ and 500tons ha⁻¹. We can infer that about 0.2 percent of the AGB values are around 200tons ha⁻¹ and 500tons ha⁻¹, meaning that most of the AGB distribution in the forest will fall around these peak values.

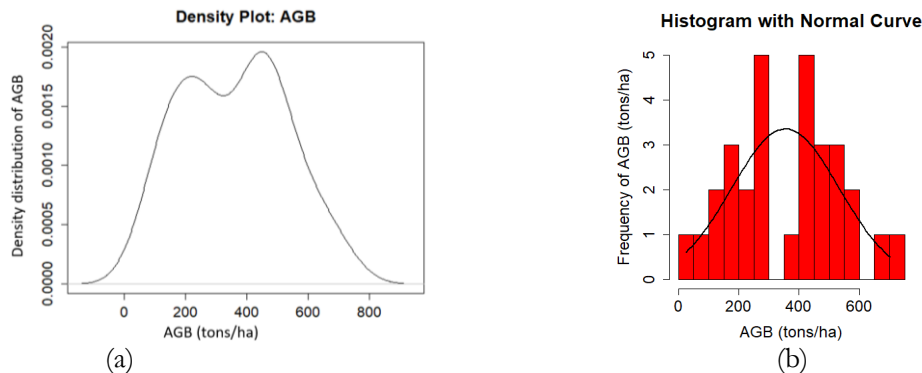


Figure 20: Density and Histogram plots showing the distribution of AGB in the Study Area. (a) Density plot (b) Histogram fitted with normal curve.

4.2. Statistical analysis of HV radar backscatter

The statistical analysis of field plot backscatter was done to understand its distribution when compared to AGB distribution in Figure 21. The trend is observed to be reasonably similar and close to a normal distribution (Figure 21b). From the backscatter density plot (Figure 21a), we can infer that about 0.15 and 0.2 percent of the backscatters from the forest falls at around -15dB and -13dB respectively. Also, backscatter analysis in height direction (with respect to LiDAR height) shows that most of the higher signal backscatter are originating from the ground layer and top canopy layer (28m to 47m) Figure 21c. This implies the effect of ground scatter to AGB estimation as ground signals may be contributing to increases in backscatter signal(value) in areas with low AGB values (saturation). Thus, Figure 21c gives us an understanding of the forest canopy level contributing more signal/backscatters used for modelling AGB. Most of the signal are observed to come from the ground and upper forest canopy.

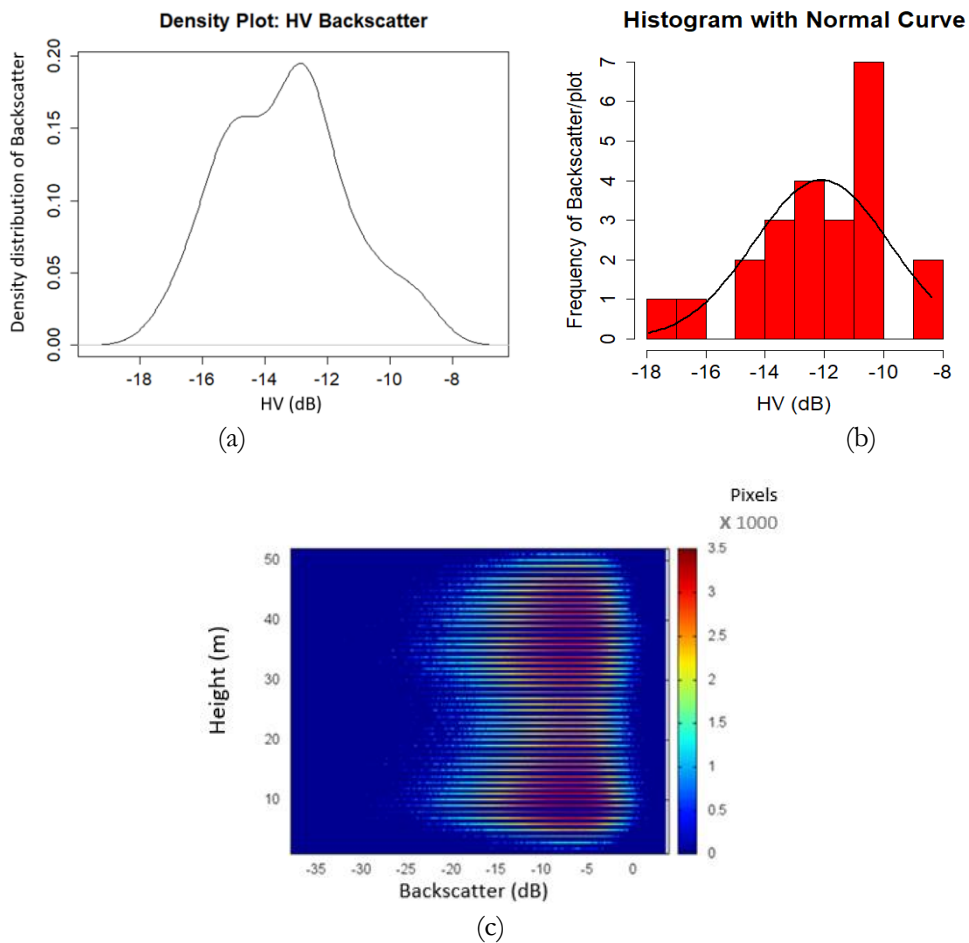


Figure 21: The density plot, the frequency distribution of backscatters and vertical distribution of backscatters in height direction. (a) Density plot of HV backscatter. (b) Histogram of the frequency distribution of backscatter (c) HV backscatter vertical distribution vs trees height.

4.3. The relationship between AGB and L-band cross polarised radar backscatters

The relationship between AGB and L-band HV radar backscatter is analysed based on the Pearson product moment correlation coefficient and regression analysis. Based on regression analysis; the linear regression, logarithmic regression were applied, and the regression equation with highest R^2 was selected for further analysis.

Based on the Pearson product moment correlation analysis (r), the result shows that AGB is correlated with HV radar backscatters with $r=0.932 \approx 93\%$ at 95% confidence interval (Figure 22).

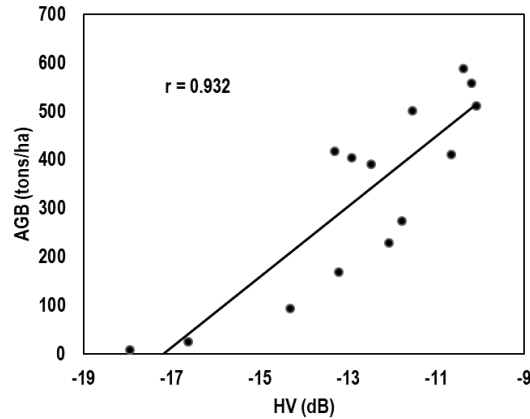


Figure 22: Scatter plot of the correlation between the cross-polarised backscatter and the Above Ground Biomass.

Two regression models, the linear and logarithmic regression models were used to analyse the relationship between AGB and HV backscatters to estimate the above-ground biomass. The linear regression model was having low R^2 of 0.76 with root mean square error (RMSE) of 92.2 tons ha^{-1} as compared to R^2 of 0.87 and root mean square (RMSE) of 68 tons ha^{-1} resulted from the logarithmic regression model respectively (Figure 23). A simple linear regression model and logarithmic regression model summary are given in Table 5 and 6.

Table 5: Summary statistics of the linear regression model of AGB and HV backscatters.

Regression Statistics					
Multiple R		0.871351			
R Square		0.759253			
Adjusted R Square		0.73919			
Standard Error		99.71194			
Observations		14			
ANOVA					
	<i>df</i>	<i>SS</i>	<i>MS</i>	<i>F</i>	<i>Significance F</i>
Regression	1	376270.6	376270.6	37.84477	4.93E-05
Residual	12	119309.7	9942.471		
Total	13	495580.2			
	<i>Coefficients</i>	<i>Standard_Error</i>	<i>t Stat</i>	<i>P-value</i>	
Intercept	1247.049	151.9197	8.208606	2.89E-06	
HV (dB)	72.5649	11.7957	6.15181	4.93E-05	

Table 6: Summary statistics of the logarithmic regression model of AGB and HV backscatters.

Regression Statistics					
Multiple R	0.932257				
R Square	0.869104				
Adjusted R Square	0.858196				
Standard Error	0.206864				
Observations	14				
ANOVA					
	<i>df</i>	<i>SS</i>	<i>MS</i>	<i>F</i>	<i>Significance F</i>
Regression	1	3.409536	3.409536	79.67583	1.2E-06
Residual	12	0.513511	0.042793		
Total	13	3.923048			
	<i>Coefficients</i>	<i>Standard_Error</i>	<i>t Stat</i>	<i>P-value</i>	
Intercept	5.103857	0.315175	16.19374	1.61E-09	
HV09	0.218436	0.024472	8.926132	1.2E-06	

The regression results explain that most of the variation in AGB is explained by the backscatter using the logarithmic regression model at 87% as compared to 76% variation explained by the linear regression model at a significant level of <0.05. In addition to that 13% and 24% of the AGB variation cannot be explained by the backscatter using the logarithmic and linear regression model effectively. Thus, for this study the logarithmic regression model, equation 12 was opted for further analysis and AGB estimation.

Equation 12: Inverted logarithmic equation for AGB estimation

$$AGB = \text{EXP} [(HV_{dB} + 21.967) / 1.728]$$

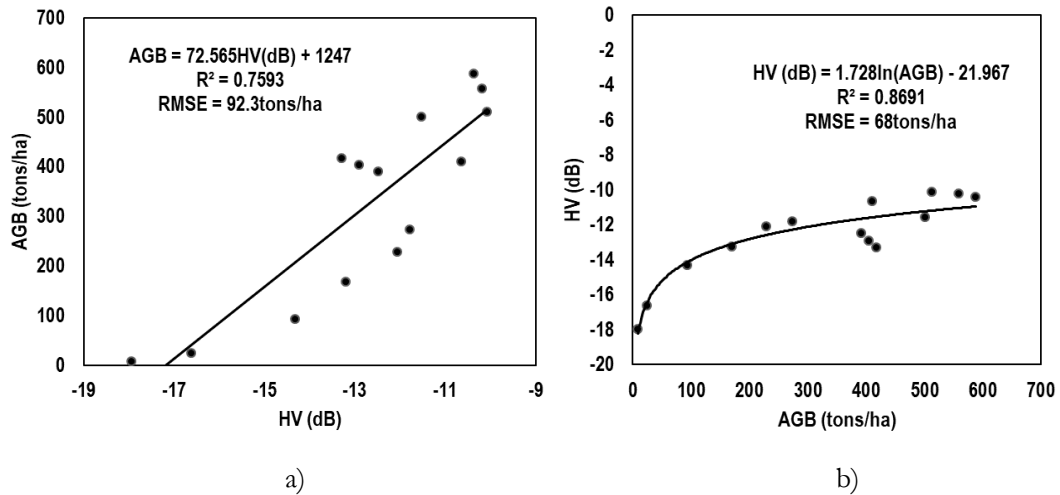


Figure 23: The scatter plot of the regression line between the cross-polarised backscatter and the above-ground biomass. a) Linear regression. b) Logarithmic regression.

4.4. The saturation point of the above-ground biomass in relation to L-band cross polarised radar backscatters

The results of the regression Analysis between AGB and cross-polarised backscatters shows that, the AGB exhibit a logarithmic relationship with the Radar backscatters at higher biomass values. The AGB obtained from field data were ranging from 8.7 to 701tons ha⁻¹, and the saturation point at which the slope was equal to 0.02dB were estimated to be at 270tons ha⁻¹. Thus, in this study, it was determined that the SAR Signal saturate at the AGB of 270tons ha⁻¹ as plotted in Figure 24.

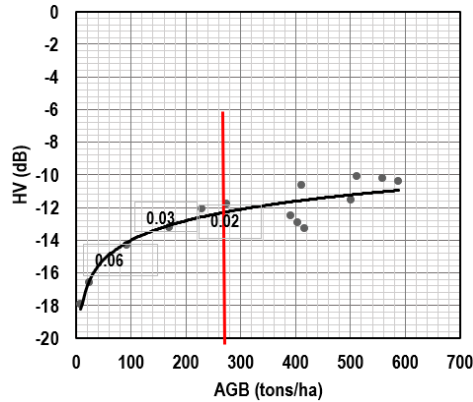


Figure 24: The graph showing the AGB saturation point with respect to the SAR backscatter. The red vertical line intersecting the AGB axis shows the estimated saturation point (slope=0.02dB).

4.5. Model validation and accuracy assessment

4.5.1. Validation data

On measuring the predictive accuracy of the developed regression model, 40% of the dataset (9 plots) were used for model validation. The dataset used for validation were independent of the 14 plots (60%) data for model development. Appendix 1, Table A and B shows the data used for developing the model and validation.

4.5.2. Model validation and accuracy assessment

The regression results of the validation between the observed and estimated AGB was having an R² of 0.8 and 0.78 using logarithmic and linear regression models respectively as shown in Figure 25. The estimated AGB explains about 80% of the observed AGB when using the logarithmic model. The predicted AGB was scaled to log10.

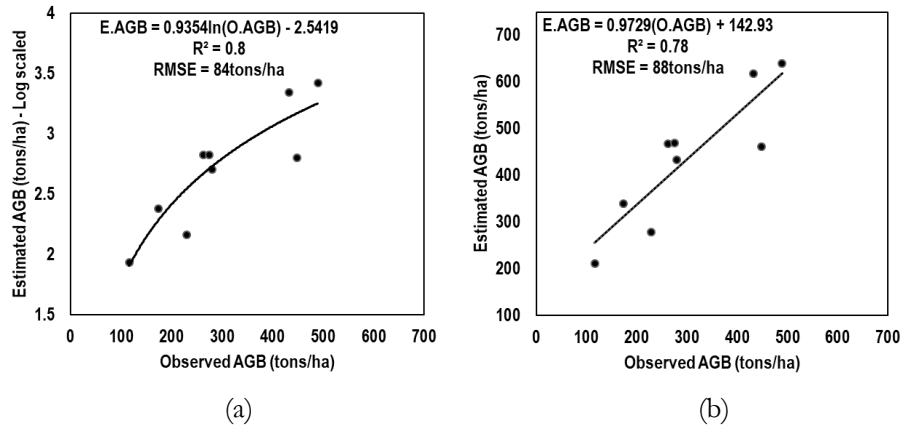


Figure 25: The scatter plots to check model validity, the predicted AGB on the y-axis and observed AGB on the x-axis. (a) Logarithmic model (b) Linear regression model

4.6. The relationship between AGB and time series of L-band polarised radar backscatters, and its influence on carbon stock sequestration estimation

The results of the time series analysis of the relationship between AGB and L-band cross-polarised radar data are as follows; Two models were developed based on multi-temporal backscatter images of 9/2016 and 9/2017 (appendix 6). The first model was developed based on the analysis of the september 2016 backscatter image, which resulted in an R^2 and RMSE of ($R^2 \approx 0.77$, $RMSE \approx 90.23\text{ton ha}^{-1}$) and ($R^2 \approx 0.82$, $RMSE \approx 79.8\text{ton ha}^{-1}$) for linear regression and logarithmic regression respectively. From these model results, the logarithmic regression was selected for use in further AGB analysis (Figure 26). The model was significant at 95% and 99% confidence interval (Table 7). The summary statistics of linear regression between AGB and backscatter for 2016 image is shown in Appendix 2. The second model based on September 2017 backscatter image was developed as mentioned in section 4.3. The model results from the two regressions show an increase in the logarithmic relationship between AGB and HV backscatter from september 2016 to september 2017. Apart from that, we tried also to develop a model to estimate AGB using backscatters from a 28 January 2017 backscatter image (appendix 6). However, the resulting models had a low accuracy in terms of $R^2 \approx 0.6$, 0.53 and $RMSE \approx 119$, 129tons ha^{-1} for linear and logarithmic regression respectively, thus it was not used further for AGB estimation, its regression results are as shown in Appendix 3.

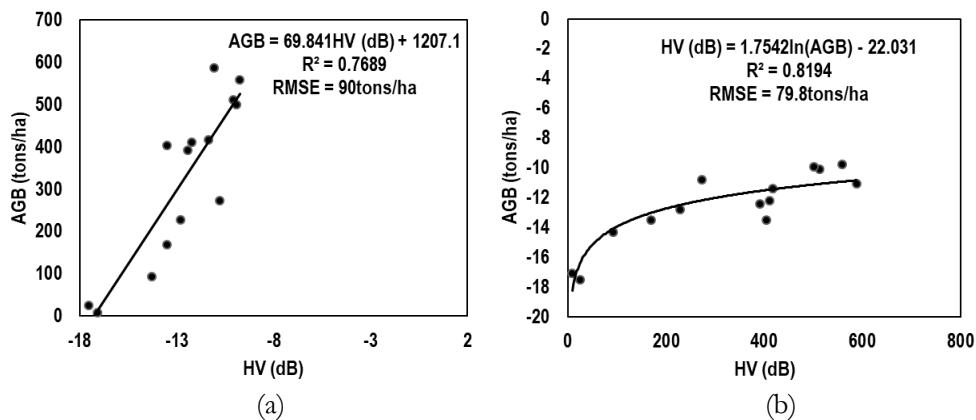


Figure 26: The scatter plots of the regression line between the september 2016 cross-polarised backscatter values and the above-ground biomass. a) Linear regression. b) Logarithmic regression.

Table 7: Summary statistics of the logarithmic regression model of AGB and time series of cross polarised radar image of september 2016.

Regression Statistics					
Multiple R	0.905207				
R Square	0.8194				
Adjusted R Square	0.80435				
Standard Error	0.242985				
Observations	14				
ANOVA					
	<i>df</i>	<i>SS</i>	<i>MS</i>	<i>F</i>	<i>Significance F</i>
Regression	1	3.214547	3.214547	54.44532	8.52E-06
Residual	12	0.708501	0.059042		
Total	13	3.923048			
	<i>Coefficients</i>	<i>Standard Error</i>	<i>t Stat</i>	<i>P-value</i>	
Intercept	4.890707	0.352506	13.87411	9.45E-09	
HV Sep 2016	0.202858	0.027492	7.378707	8.52E-06	

On the other hand, the first (2016) model was used to estimate AGB and carbon stock for the study area subset backscatter image of September 2016 and September 2017, and their average AGB were estimated to be 192.69ton ha⁻¹ and 199.95ton ha⁻¹ respectively. Again, the second model was applied on September 2017 subset image which resulted in an average AGB of 199.93ton ha⁻¹ which shows a little difference in estimated Average AGB between the two models. Taking the difference between the two-year average estimated AGB between the images subset AGB, resulted in AGB difference of 7.24ton ha⁻¹ which is equal to an increase of 3.62ton ha⁻¹ of carbon stock between the year interval, september (2016/2017) (Table 8). From this result, we can say that carbon sequestered from the atmosphere for the period september 2016 to September 2017 was 3.62ton ha⁻¹. Figure 27 shows the carbon stock estimated using the subset from a study area between the year (2016/2017), and the corresponding sequestered carbon.

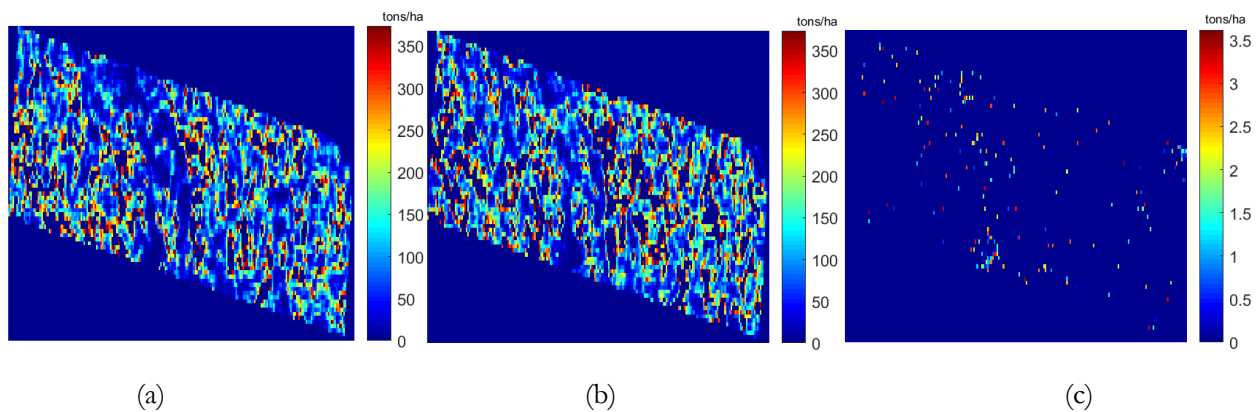


Figure 27: Carbon stock of the subset study area for the year september 2016/ 2017 and the corresponding sequestered carbon. (a)Carbon stock september 2016 (b)Carbon stock september 2017 (c) Sequestered carbon stock.

Table 8: The average amount of AGB/carbon stock from the subset and the sequestered carbon

Parameters	Average AGB (tons/ha)	Average Carbon Stock (tons/ha)
September 2016	192.69	96.35
September 2017	199.93	99.97
Change in AGB & Carbon Stock/year	7.24	3.62

4.7. The relationship between AGB and a combined L-band HV, HH polarised radar backscatter in relation to single HV backscatter

The multiple regression results (Table 9) of a model between AGB and HV, HH polarised radar backscatter shows a 1% increase in the linear and logarithmic relationship between AGB and HV, HH backscatter. We obtained an increase of $R^2 \approx 0.77, 0.88$ compared to $R^2 \approx 0.76, 0.87$ obtained when using only cross polarised backscatter (HV) to derive the relationship in section 4.3, for both linear and logarithmic regression respectively. The multiple regression approach of combining HV and HH polarised backscatters did not add a significant improvement in R^2 and RMSE results for AGB estimation with reference to the model developed using only cross-polarized backscatter (Table 10). In fact, the addition of HH to the model did not have a significant effect on AGB/carbon stock estimation at 95% confidence interval (p-value for HH was greater than 0.05).

Table 9: Summary statistics of the multiple logarithmic regression model of AGB and HV, HH polarised radar backscatter.

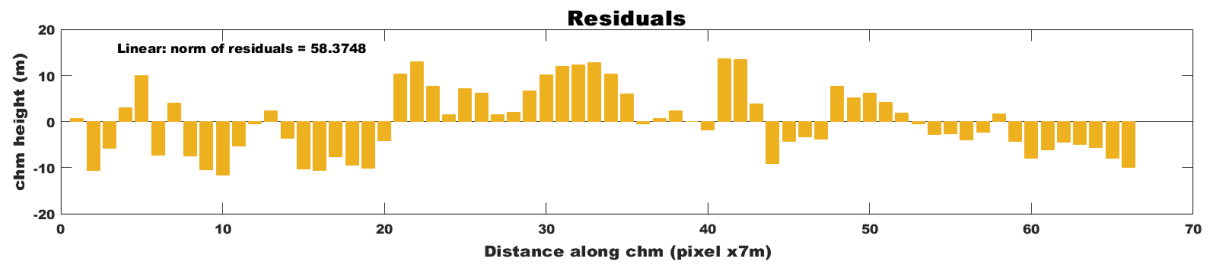
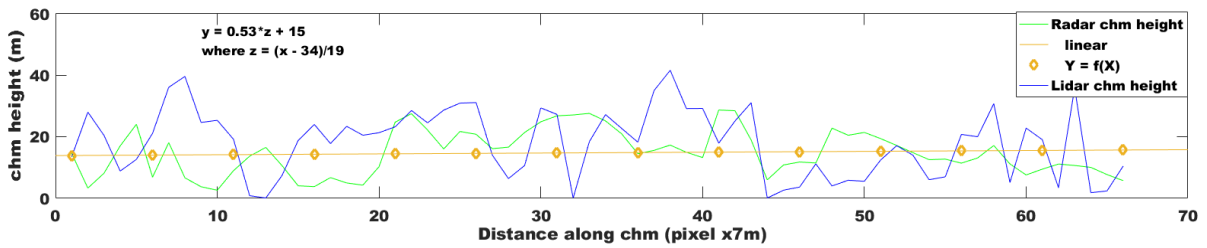
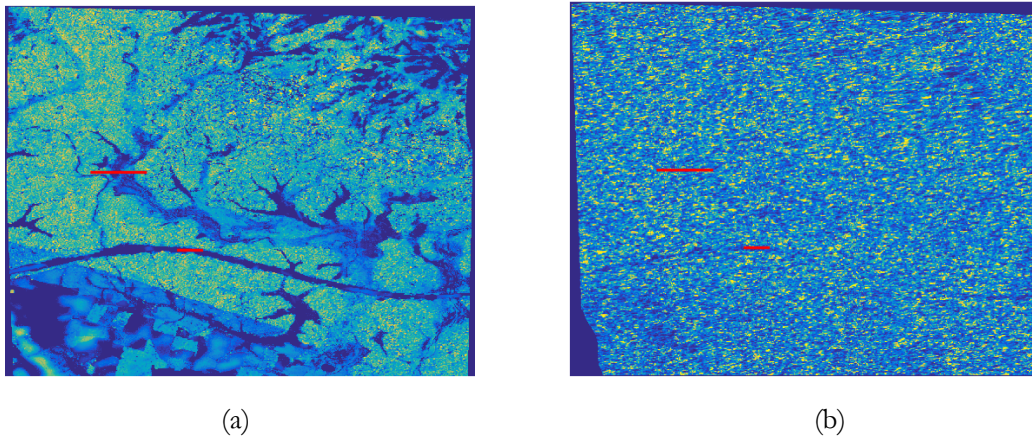
Regression Statistics					
Multiple R	0.935421				
R Square	0.875012				
Adjusted R Square	0.852287				
Standard Error	0.21113				
Observations	14				
ANOVA					
	<i>df</i>	<i>SS</i>	<i>MS</i>	<i>F</i>	<i>Significance F</i>
Regression	2	3.432714	1.716357	38.50424	1.08E-05
Residual	11	0.490334	0.044576		
Total	13	3.923048			
	<i>Coefficients</i>	<i>Standard_Error</i>	<i>t Stat</i>	<i>P-value</i>	
Intercept	5.15909	0.330668	15.60201	7.53E-09	
HV	0.199644	0.036096	5.530876	0.000178	
HH	0.02924	0.040551	0.721082	0.485902	

Table 10: Comparison of the cross polarised radar backscatter logarithmic regression model and multiple logarithmic regression model of the cross and like polarised radar backscatter.

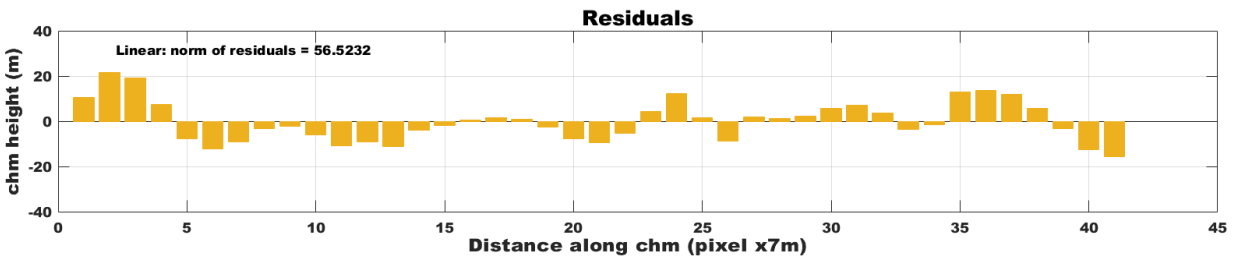
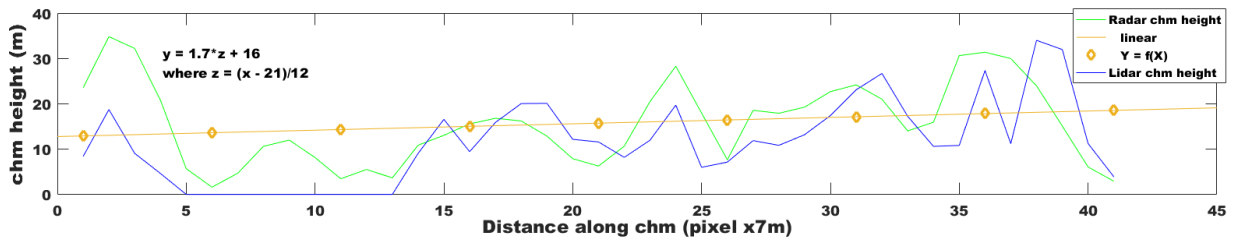
Model type	R ²	RMSE (tons ha ⁻¹)
AGB & HV model	0.87	68
AGB & HV, HH model	0.88	65

4.8. Interferometric height results

In this section, the interferometric phase and thus the elevation information in the interferometric images are analysed. Figure 28 shows the height maps generated from LiDAR data (Figure 28a) and ALOS-2 PALSAR-2 image (Figure 28b) of the study area. The interferometric forest height (Canopy Height Model) CHM map was produced using one method; DEM differencing inversion algorithm (Figure 28b). When comparing the height images, it can be observed that both height maps give a roughly similar estimation of the height tendencies at the study area which compare somewhat well with the reference data (LiDAR data).



(c)



(d)

Figure 28: (c) and (d) Height profile line and its residuals drawn over (a) LiDAR CHM (b) Radar CHM derived by use of DEM differencing algorithm.

Studying the height variations in more detail a line of same length and location drew on the LiDAR and radar CHM (red lines) Figure 28a, and b respectively and, their values are represented on a 2D plot (Figure 28c and d). Forest height on the y-axis and distance along the ground on the x-axis. Height from LiDAR CHM is presented in blue line and height from radar CHM are presented in green (Figure 28c, d). From the profile plot, it can be observed that the height tendency follows the same pattern on both CHM. The differences can also be observed in interferometric height estimated using the radar data is higher than the LiDAR CHM. The radar CHM height estimated using a DEM difference inversion algorithm shows a minimum variation with LiDAR CHM showing that height from L-band ALOS-2 PALSAR-2 interferometry can be used for AGB estimation. It is also important to note that, the ALS height data were acquired in 2014 while the ALOS-2 PALSAR-2 were acquired in 2017, this poses a significant difference in height difference that exists between the data.

4.8.1. The relationship between LiDAR-derived CHM height and radar-derived CHM height

A scatter plot (Figure 29) of the average plot height from interferometry and LiDAR is drawn to show the relationship that exists between the height estimated from the two-data type. The coefficient of determination (R^2), Pearson correlation coefficient (r) and root mean square error (RMSE) of the height from the two chm is 0.56, 0.75 and 4m respectively. The height pattern shows the existence of a linear relationship between the two heights retrieved from both datasets.

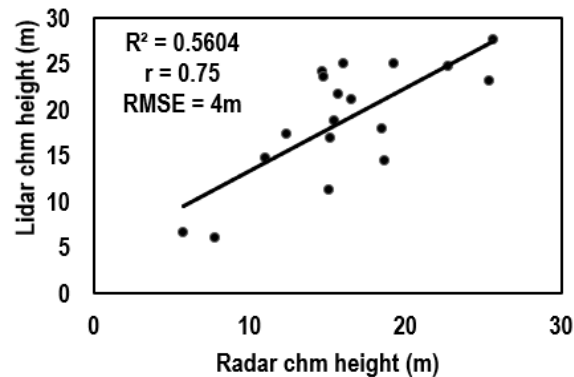


Figure 29: A scatter plot showing the SAR interferometric height distribution in relation to height derived from LiDAR data.

4.9. Tomographic distribution of the L-band cross polarised radar backscatters in relation to AGB

Fourier analysis was used for tomographic reconstruction of backscatter in height direction for a given range of pixels. The SAR signals are observed to be distributed in the ground and upper forest canopies (Figure 30b). However, the distribution is not constant due to the forest structure variation as seen in Figure 30a. We can also observe that, in dense forest areas stronger scattering amplitude is visible in the canopy compared to less/non-vegetated areas where ground scattering dominates (Figure 30b). Ground backscatters are observed because of SAR signal penetration below the canopy and signals from open areas. These results proves that, tomography can be effective in AGB/carbon analysis.

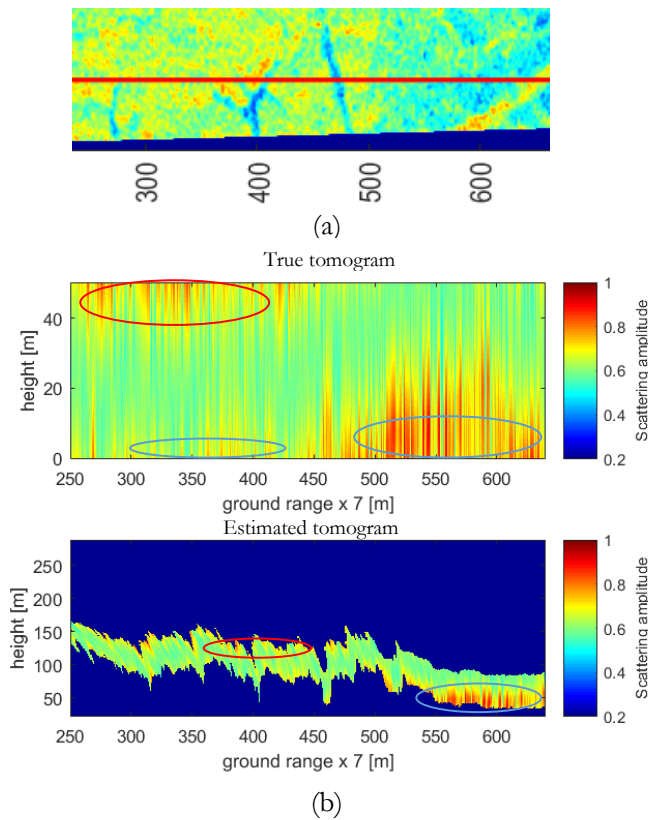


Figure 30: Vertical tomographic slice. (b) of backscatter variation through forest canopy through azimuth red line (a). The backscatter intensity increases from green to red. The red line in (a) shows the test slice used in the analysis. Through the profile, it is easy to distinguish the scattering contribution (ground scatters-blue circle, canopy scatters-red circle).

4.9.1. Vertical distribution of HV backscatter in relation to height estimated from DEM differencing algorithm

The scatter plot (Figure 31) shows the backscatter distribution in relation to interferometric phase height obtained using DEM differencing of HV, HH ALOS-2 PALSAR-2 interferometric images. Most of the high backscatter power (red color in Figure 31) scattering mechanisms are observed to fall in the lower forest layer (ground layer). The ground scatters are known to have an effect in determining the relationship between the backscatter from the forest and AGB.

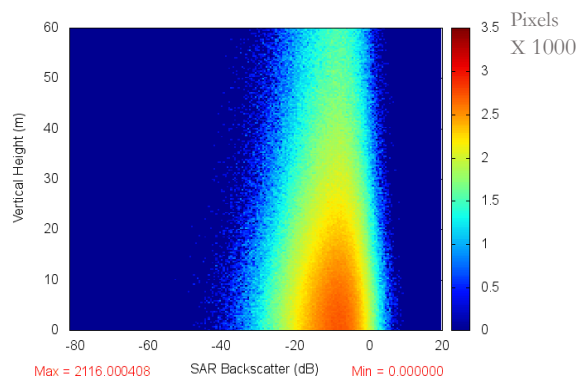


Figure 31: Scatter plot of the HV backscatter distribution in relation to DEM differencing interferometric height.

4.10. Estimated AGB and carbon stock of the study area

The study area AGB and carbon stock estimation were done using inversed logarithmic models developed in section 3.6.6, Table 3 - model 1 and 2 as shown in Figure 32, 33a and b respectively. The AGB were estimated based on the logarithmic model developed by the existing relationship between AGB and cross-polarised backscatter. The estimated AGB were converted to carbon stock using a conversion factor of 0.5 (Hirata *et al.*, 2012). The total AGB and carbon stock for the study area was estimated to be (AGB \approx 282770tons, carbon \approx 141385tons) and (AGB \approx 285930tons carbon \approx 142965tons for September 2016 and September 2017 respectively.

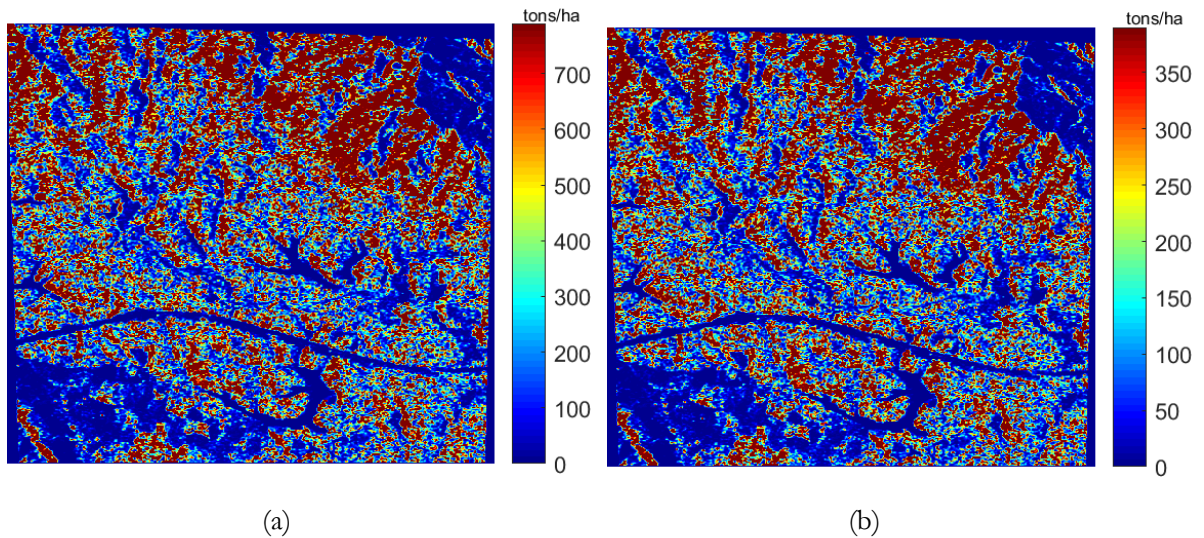


Figure 32: Distribution of AGB and carbon stock in the study area as of september 2016. (a) AGB distribution (b) Forest carbon stock distribution

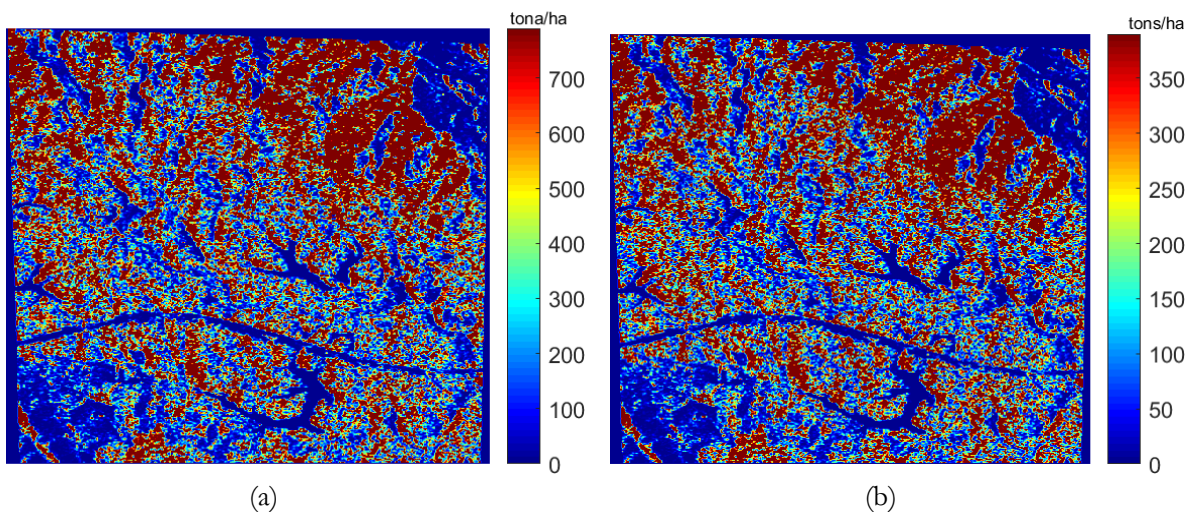


Figure 33: Distribution of AGB and carbon stock in the study area as of september 2017. (a) AGB distribution (b) Forest carbon stock distribution

5. DISCUSSION

5.1. The Relationship between AGB and L-band cross polarized radar backscatters

In this study, we used 23 field plots from the study area. Out of 23 plots, 14 plots were used for model development, and the remaining 9 plots were used for model validation. The relationship between the cross-polarised backscatter and the AGB were assessed using linear and logarithmic regression analysis.

In the meantime, the window size of 5 x 5 pixels, were used to retrieve average backscatter values for each field plot, the retrieved average backscatter was correlated with the selected observed field AGB plots (14 plots) for model development. A strong relationship (r) of $0.932 \approx 0.93$ was observed between the cross-polarised backscatter and AGB at a significant level of 95% and 99%, meaning that the SAR backscatter responds well to AGB increase and can be used to estimate AGB. The same trend of relationship can also be seen in density plot figure 20(a) and 21(a), where the AGB and backscatter distribution follow the same pattern.

Consequently, further analysis using regression technique was done to assess the relationship between cross-polarised backscatter and AGB. According to the regression results, the linear regression analysis appeared to show a moderate relationship between cross-polarised backscatter and AGB than using logarithmic regression with R^2 of 0.76 and 0.87 respectively. It shows that 76% and 87% of the variation in AGB are explained by the cross-polarised backscatter, leaving out 24% and 13% unexplained variation in AGB using linear and logarithmic model respectively. These results indicate that the logarithmic regression model is a more appropriate candidate for modelling the AGB as it has higher R^2 compared to the linear regression model. Moreover, looking at Figure 23 (b) in comparison to Figure 23 (a) and the behaviour of the data points is a proof that logarithmic regression best fit and represent such a relationship better than the linear regression. Almost similar results were achieved by Hamdan et al. (2011) in Malaysian tropical forest not so far from Berkelah in which they show that the best model fit the relationship between AGB and ALOS PALSAR L-band HV polarised backscatter was the logarithmic regression. Their scatterplot looks almost the one presented by this study (Figure 34). Moreover, their R^2 is very close to the one achieved in this study. However, a study done by Sumareke, 2016 showed that AGB is highly related with cross-polarised backscatter using linear regression with R^2 of 0.817 which contrary to our results. The reason for the difference is attributed to the AGB ranges in their study $60.16 - 367.07 \text{ton ha}^{-1}$ as opposed to our study AGB range $8.7 - 700 \text{ton ha}^{-1}$. In another study by Mitchard et al. (2009) which was done in tropical Africa to assess AGB using ALOS PALSAR L-band HV polarisation, they found out that logarithmic regression relationship is the most appropriate to characterise the such a relationship. Their R^2 was close to the one that this study has come up with (Figure 35).

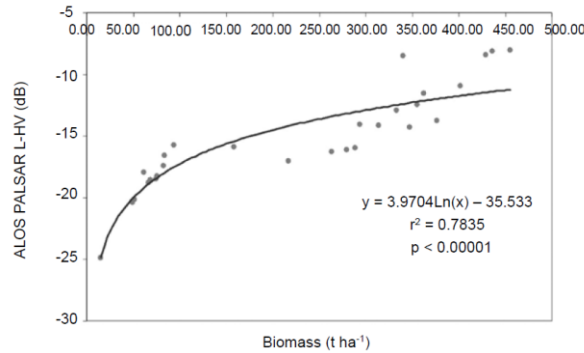


Figure 34. The scatter plot of the logarithmic regression of AGB and ALOS PALSAR L-band HV polarisation by Hamdan et al. (2011) in tropical rainforest of Malaysia.

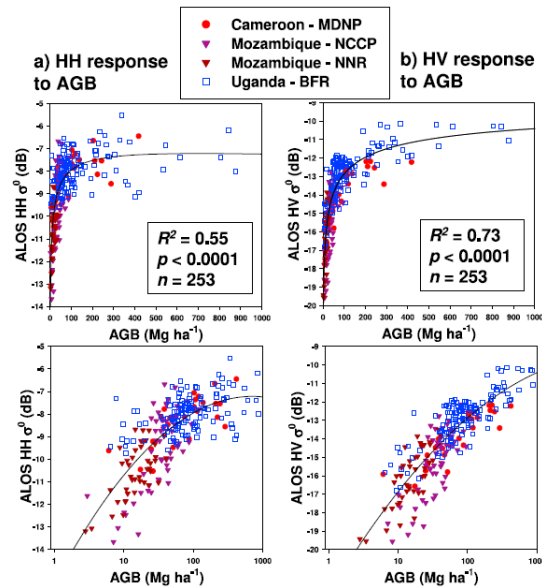


Figure 35. From Mitchard et al. (2009) ALOS PALSAR (a) HH and (b) HV backscatter in 4 locations of African tropical forest in which radar backscatter plotted against field-measured AGB (Mg/ha) for all four sites combined, with the x-axes shown with conventional and log₁₀ scales.

5.2. Biomass saturation

Despite having practically, a good relationship between the SAR backscatter and AGB, the predictive capability of the SAR backscatter tends to level off at 270 tons ha⁻¹ (Figure 24). Essentially after this point, the regression line did not shift appreciably upward. Instead, a decreasing trend of the backscatter as AGB increased was observed.

The reason for Biomass saturation can be explained as:

Moisture content: The reason for saturation are associated with varying moisture content in the forest which reduces the signal strength of the backscatter particularly from ground trunk interaction at higher AGB (Imhoff, 1995).

Forest structure variation: Areas with low AGB (vegetation) and canopy gaps (sparse vegetation) increases the power signal reflected to the sensor causing an increase in AGB. According to Hamdan *et al.*, (2015), a good result from L-band Palsar data can be obtained when the backscatter interacts with forest canopies, as opposed to when the backscatter is a mixture of canopy and ground reflection.

Similar AGB saturation results were obtained from the research done by Hamdan *et al.*, (2015) for determining L-band saturation level for AGB of dipterocarp forests in Peninsular Malaysia, where a saturation point of 200tons ha⁻¹ was estimated. AGB was observed to increase rapidly at low AGB level up to (<200tons ha⁻¹) with R² of 0.7558 and decrease at higher AGB values (>200tons ha⁻¹) R² of 0.0264. Moreover, when all AGB values were combined the overall R² decreased to 0.3553. Other studies also reported that AGB saturation occurs at 120.7tons ha⁻¹ for boreal forest (Suzuki *et al.*, 2013), 40 tons ha⁻¹ for Broadleaf evergreen forest at L-band (Figure 35) (Imhoff, 1995), which is lower than our predicted saturation point. A study by Yu & Saatchi, (2016) reported the average saturation level for AGB estimation from different forest types using HV backscatter to be ≥100tons ha⁻¹, the forest types were Tropical Moist Broadleaf, Temperate Broadleaf/Mixed, Temperate Conifer, Tropical Savanna/Shrub, Tropical Dry Broadleaf, Boreal + Tundra.

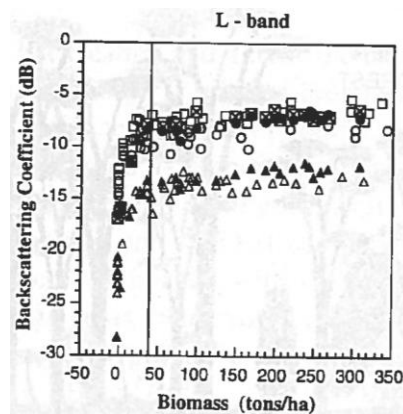


Figure 36: L-band backscatter saturation at lower AGB values. (As adopted from Imhoff, 1995)

According to Mitchard *et al.* (2009) “radar backscatter response saturates at higher biomass values in savanna ecosystems, at a variable point (>60 Mg ha⁻¹, >80 Mg/ha, and >150 Mg/ha, all using different L-band systems). This saturation point is due to the competing mechanisms of scattering and attenuation (absorption) of microwave energy in the canopy of the vegetation, and it is highly dependent on the canopy density, stem density, tree species, and vegetation and soil moisture conditions, as well as the characteristics of the radar data used. Nevertheless, this point is high enough that useful biomass estimates are possible for mixed tree-grass systems (savannas and woodlands), as these typically have maximum AGB values <100 Mg/ha, though higher values can exist in gallery forests (Brown, 1997)”.

In addition to that, a study was done by Hamdan *et al.*, (2015) on L-band saturation level for above ground biomass of dipterocarp forests in Peninsular Malaysia. They revealed that AGB estimation with higher AGB values has a weaker relationship with cross-polarised backscatter; they obtained (R² of 0.0264) at AGB values >200Mg ha⁻¹. The decline in the correlation between AGB and the SAR Backscatter is attributed to unstable scatters or signals coming from higher AGB values (Le Toan *et al.*, 2004).

The existence of a logarithmic relation between the L-band backscatter and AGB is due to the radar signal saturation as they are reflected from the forest. This saturation effect is more profound in mature forest stands which have higher canopy cover and higher amount of AGB than in growing forest (Imhoff, 1995).

5.3. The Relationship between AGB and time series of L-band polarized backscatters and its influence on carbon stock sequestration estimation

This section explored the effectiveness of using multi-temporal L-band Polarized Radar images in modelling AGB, essentially by deriving its relationship with AGB and Estimation of the amount of sequestered carbon in a year period. The results indicated existence of higher relationships between AGB and time series L-band Polarized Radar Backscatters (section 4.6). However, there was also an increase in R^2 from 0.82 up to 0.87 and a decrease in RMSE from 79.8ton ha⁻¹ to 68ton ha⁻¹, using logarithmic regression for September 2016 to September 2017 SAR backscatters respectively, indicating an increase in AGB/carbon stock in the study area. However the simple linear regression analysis resulted in a decrease in R^2 from 0.82 up to 0.87, this decrease is attributed to saturation effect of the backscatter to higher AGB values (Hamdan *et al.*, 2015). Thus, logarithmic regression was preferred for AGB/carbon stock estimation and carbon sequestration estimation because it responds well to the saturation trend, hence better estimates can be made. From this study, it was also found that, the average amount of AGB estimated increased from 192.69tons ha⁻¹ in September 2016 to 199.93tons ha⁻¹ in September 2017. These results paved the way for calculating the amount of carbon sequestered in a year period by the forest using a subset from the study area. A total of 3.62ton ha⁻¹ was determined as the amount of carbon sequestered by the forest from September 2016 to September 2017.

The results of the amount of sequestered carbon from this study are related to similar studies done by Fan *et al.*, (1998) and Malhi *et al.*, (1999), wherein their studies they found that tropical rainforest carbon sequestration rate ranges about 2.0 to 5.9 t C ha⁻¹ per year. In their studies, they also indicated that the carbon sequestration rate in a year also varies depending on the forest susceptibility to logging intensities and unpredictable hazards such as forest fires.

On the other hand, we tried to incorporate the SAR image acquired in January 2017 for the backscatter analysis in relation to AGB. However, the relationship resulted in a substantial decrease in R^2 to 0.53 and 0.6 and an increase in RMSE to 129tons ha⁻¹, 119tons ha⁻¹ for logarithmic and linear regression respectively. The decrease is attributed to environmental condition effect (moisture) introduced by long time rainfall over the study area (October to January) resulting in high backscatter signal to be recorded. As it can be noted in Figure 36 (blue-line-January 2017 image) the backscatter variation at a given point exists between different time periods of SAR data acquisition. The images acquired in September are similar or correlated with low backscatter values as opposed to the January backscatter image which has relatively abnormal high backscatter values over the same forest plots. The reason for this is attributed to soil moisture variation over different time periods; higher moisture content has an influence on backscatter resulting in more of surface scattering than volume scattering which is highly related to AGB. Also, a study was done by Wang *et al.*, (1992) reported a backscatter value increase of 5dB and 3dB with an increase in soil moisture for both low and AGB vegetation respectively. Appendix 5 shows the average precipitation variation in the study area.

From this study, we can see that it is possible to estimate the amount of sequestered carbon provided that data be acquired on the given month interval while avoiding influence from environmental factors (moisture in this case). The strength of the model used for carbon sequestration estimation relies on the fact that, the two image backscatter data were acquired almost exactly the same period. Moreover, the SAR backscatter

cross-polarisation used includes volume scattering which relates closely to AGB, thus making it possible to achieve the results (Antropov *et al.*, 2017).

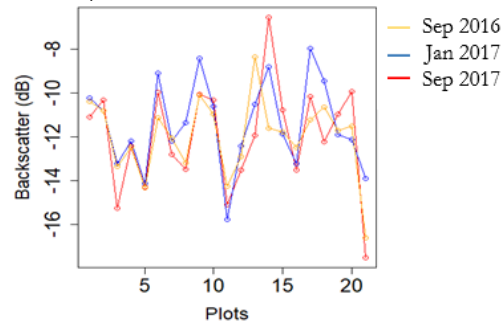


Figure 37: Temporal backscatter distribution from the field plots. (The orange and red line represents backscatter of September 2016 and 2017 images respectively; the blue line represents the backscatters from January image).

5.4. The relationship between AGB and a combined L-band HV, HH polarised radar backscatter in relation to single HV backscatter

On analysing the relationship between AGB and dual polarised backscatters (HV, HH), resulted in an R^2 of 0.88 and RMSE of 65tons ha^{-1} which is an increase in R^2 , for 1% difference from the lone HV model. However, this result did not achieve a significant improvement in R^2 when compared to the AGB model developed using only HV backscatters with R^2 of 0.87, RMSE 68tons ha^{-1} . The multiple regression model did not achieve significant improvement because the added HH variable was not significant at p-value 0.95 or 0.95, meaning that the estimated AGB using the multiple regression model are significantly different from the observed AGB values. The reason for this is attributed to surface scattering characteristics of HH backscatters as opposed to volume scattering of HV backscatters (Antropov *et al.*, 2017). The result of this study differs from a study by Sumareke, (2016) which suggested that addition of HH backscatter would have promising improvement in R^2 and eventually AGB modelling.

5.5. The relationship between interferometric forest height and LiDAR forest height

The comparison of the relationship between interferometric forest height from model inversion heights and LiDAR forest height was found to have a correlation coefficient $r \approx 0.75$, $R^2 \approx 0.56$ and the RMSE of 4m at 95% significance level. The relationship was interpreted as a moderate relationship. The moderate relationship between the Interferometric height and LiDAR height is attributed to low coherence (Figure 37) and phase noise which causes errors in the phase unwrapping process and eventually height retrieval (Lee *et al.*, 2013).

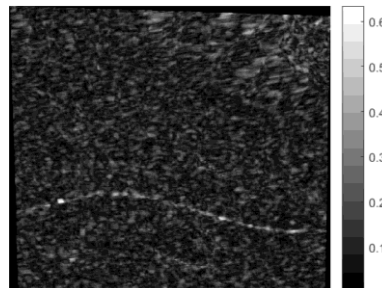


Figure 38: Coherence phase variation in the study area. The study area is dominated by low coherence values ranging from 0.1 to 0.6, posing errors in forest height retrieval.

These results, agreed with the study done by Lei & Siqueira, (2014) on the estimation of forest height using spaceborne repeat-pass L-band InSAR correlation magnitude over the US State of Maine. Were they obtained $R \approx 0.58, 0.49$ and $RMSE \approx 3.6, 3.9$ using images of different dates 07/10/2007 to 08/25/2007 and 07/10/2007 to 10/10/2007 respectively (Figure 38). The InSAR height correlation was affected by temporal decorrelation and poor signal to noise ratio as a result of ground scattering.

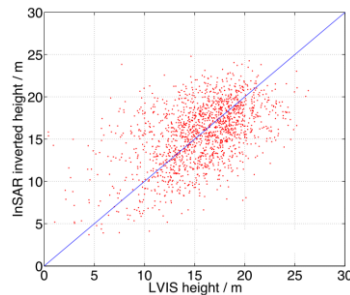


Figure 39: A quantitative comparison of ALOS InSAR inverted height and LiDAR height. (As adopted from Lei & Siqueira, 2014)

Generally speaking height estimates from L-band InSAR applications has been successfully obtained when using airborne InSAR images with short temporal baselines, i.e. 40 min (Lei & Siqueira, 2014). The L-band ALOS-2 PALSAR-2 data used for this study was having a temporal gap of up to 7 months which poses an increase in temporal decorrelation effect, which results in the low coherence of signals from the forest. The low coherence is attributed to the change in vegetation and environmental conditions such as tree growth, wind, moisture.

5.6. The relationship between tomographic backscatter layers and AGB

According to Reigber & Moreira., (2000) SAR tomography is a multibaseline interferometry which requires number of tracks to be greater than two. On tomographic imaging done by Cloude, (2007), he demonstrated the use of small number of baseline (dual baseline coherence tomography) for tomographic retrieval of forest vertical structure (Figure 40), comparable to the vertical structure of backscatter distribution retrieved in this study (Figure 30). In his paper, he demonstrated tomography based on the estimation of a Fourier Legendre series, that with two baselines (N) it is possible to retrieve up to five terms of the Fourier Legendre series ($2N + 1$). Another study done by L. Li *et al.*, (2015) achieved good tomographic results using only three flight track to reconstruct the DEM and CHM of the tropical forests using SAR tomography. Urasawa *et al.*, (2016) also used three L-band Pi-SAR-L2 datasets to study the height distribution of SAR backscatter using SAR tomography analysis.

Apart from retrieving the vertical tomographic slice for understanding the backscatter distribution from forest (Figure 30). This study was also aiming to retrieve the tomographic backscatter layers at different forest heights to derive the relationship between the height layer backscatter and AGB. However, technically the data processing to retrieve backscatter image layers from the canopy was not successful due to the following reasons.

SAR tomography analysis requires a sufficient number of baseline which are regularly distributed to retrieve 3-D scatter distribution in height direction. Thus, due to the limited number of images with irregularly spaced baseline available for this study, the 3-d image reconstruction in elevation direction was not able to separate multiple scatters at different forest height positions (Lombardini & Pardini, 2008).

In addition to that, the SAR tomography analysis for forest application is still at an early experimental stage. Thus most of the 3-D SAR image reconstruction are done using airborne remote sensing images and from SAR image simulations. The experimental and simulation data usually consists desired parameters for SAR tomography analysis, making it possible to achieve accurate tomographical results (Ho Tong Minh *et al.*, 2014, 2015; Lombardini & Reigber, 2014; Lombardini & Viviani, 2014; Tebaldini, 2010; Tebaldini & Rocca, 2012). Also, software which are freely available for SAR tomography processing are still at developmental stages, thus limited for robust tomographic analysis and parameter settings, e.g. PolSarPro. In another scenario, the robust tomoSAR processing modules, tomographic processor and platform are not easily/freely available as they are still in developmental stages by the developers.

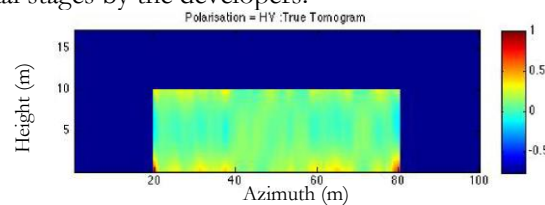


Figure 40: Azimuth tomographic slice through canopy. (As adopted from Cloude, 2006)

5.7. The research relevance for REDD+

An important aspect for REDD+ is to have a highly accurate method which can be used to estimate the AGB. From the results of this study, the L-band ALOS-2 PALSAR-2 data has greater potential to be used for AGB estimation. This is due to the potential of retrieving various forest parameters (volume, height) which can be utilised for AGB estimation and forest characterisation over the wider area. However, the L-band ALOS-2 PALSAR-2 SAR images are not freely available, which poses a limitation in the case when a larger number of images are required for processing, e.g. SAR tomography. Aside from that, the SAR backscatters have shown the potential for estimation of AGB/carbon stock and carbon sequestration estimation over a given period. Hence, this research provides a window on the use of SAR data for AGB/carbon stock and carbon sequestration estimation. SAR data can be best utilised to enable the success of REDD+ to reduce emission from the atmosphere caused by unsustainable forest management and monitoring.

5.8. Study limitations

The cost associated with the acquisition of ALOS-2 PALSAR-2 images posed a more significant disadvantage to obtaining a sufficient number of images for SAR tomography analysis of SAR images. A sufficient number of images would provide the required baselines for vertical retrieval of backscatter reflectivity's associated with the forest canopy.

GPS error associated with identification plot centre. The shift in plot centre posed difficulties in the extraction of average plot backscatter values. Hence 5m which was the GPS error was added to a plot radius on each side to retrieve the average plot backscatter. However, this process has a smoothing effect to the final average plot backscatter value.

The L-band ALOS-2 PALSAR-2 images had a gap of 7 months between image acquisition which introduces temporal decorrelation errors in forest height estimation during interferometric analysis.

Also, the ALS data used for this study were acquired in 2014, creating a gap of three years with field data collected (DBH) in 2017. This creates errors in height estimation due to tree growth and forest structure change thought to happen during the three-year gap period.

6. CONCLUSION

6.1. Conclusion

This study explored the use of ALOS-2 PALSAR-2 data for AGB/carbon stock and carbon sequestration estimation. The DBH from field and height from LiDAR data were used as reference data. The L-band ALOS-2 PALSAR-2 data were used for deriving the relationship between the SAR backscatter and AGB, which eventually resulted in a model for AGB and carbon estimation and mapping. The backscatter saturation point for AGB estimation were also analysed. We also, explored the possibility of using radar data to assess the amount of carbon sequestered in a year using time series of L-band cross polarised radar backscatter data. The relationship between interferometric height and LiDAR height were also analysed. Likewise, we assessed the distribution of backscatter in height direction, and finally, AGB and carbon stock were estimated. The following conclusions addresses the research questions based on the results achieved from this research objectives.

Research Question 1

What is the relationship between the L-band cross polarised radar backscatter values and AGB/carbon stock from TLS and ALS data?

- There is a high relationship between L-band cross polarised radar backscatter values and AGB/carbon stock with R^2 of 0.87 and RMSE of 68tons ha^{-1} . However, the relationship was a logarithmic relation were the AGB prediction increased with an increase of backscatter up-to a saturation point. The correlation analysis showed a high correlation of $r=0.932$. The high relationship was significant at 95% and 99% confidence level.
- On the other hand, addition of like polarised backscatter did not significantly improve AGB estimates at 95% and 99% confidence level.

Research Question 2

What is the saturation point of AGB estimation in relation to the L-band cross polarised radar backscatter values?

- The results of this study confirmed the presence of saturation on L-band cross-polarised SAR backscatter at the AGB of 270tons ha^{-1} . The existence of saturation can be viewed as a limitation for estimation of higher levels AGB values $>270tonsha^{-1}$. Thus, a direct linear relationship between HV backscatter and AGB may not be a correct approach to estimate AGB.

Research Question 3

Relationship between AGB and time series of L-band cross-polarized radar backscatter and its influence on carbon sequestration estimation

- A higher relationship exists when multi-temporal L-band cross-polarised SAR backscatter, are used to model the relationship between SAR data and AGB. A significant relationship was observed with R^2 of 0.82 and 0.87. The amount of carbon sequestered from September 2016 to September 2017 was estimated to be 3.62 tons ha^{-1} . From this result, we conclude that time series of SAR data can be

used to model AGB/carbon stock and eventually estimate carbon sequestration rate with reasonable accuracy.

Research Question 4

What is the relationship between forest height estimated from interferometric SAR images of ALOS-2 PALSAR-2 and ALS height?

- The correlation and regression analysis between interferometric height and LiDAR-derived height revealed a moderate relationship $r \approx 0.75$, $R^2 \approx 0.56$ and the RMSE of 4m. Besides, there was a good linear trend of height variation between the two datasets. Thus, a moderate accuracy in forest height estimation can be achieved, when L-band Alos2-Palsar-2 data are used to map forest height.

Research Question 5

What is the distribution of the L-band cross polarised radar backscatters in height direction in relation to AGB?

- By visual analysis of a tomographic profile of a slice from the L-band Alos2-Palsar-2 images, the backscatter contribution comes from both ground and canopy layers of the forest. High power signal backscatter was observed in the ground and a sub-top layer of the canopy, indicating an influence of topography on backscatter reflected to the satellite sensor hence affecting AGB estimation.

Research Question 6

What is the AGB/carbon stock estimated by L-band cross polarised radar backscatter image?

- A total of 285930tons and 142965tons of AGB and carbon was estimated for the whole study area by September 2017 respectively. The minimum and maximum AGB per ha were estimated to be 10.3tons ha⁻¹ and 970tons ha⁻¹ respectively.

6.2. Recommendation

On relationship between AGB and SAR backscatters

- When it comes to establishing the plot centre, more accurate GPS system should be used for reading and recording the plot centres as well as tree locations.

On biomass Saturation

- Models for AGB estimation with SAR backscatter achieves high accuracy and results when used in forests with low to moderate AGB values. This favours its use in low AGB forest as compared to higher AGB forest with high structure variability. In addition to that more improved algorithm as in (Ho Tong Minh et al., 2016) can be used to improve the results.

On relationship between AGB and time series of L-band polarized radar image parameters

- A number of images covering the whole year period can be acquired to do more study on the influence of time series images on AGB/carbon stock estimation and carbon sequestration. Also, preferred time of image acquisition with less effect on backscatter signal relationship with AGB can be established.

On interferometric height

- To achieve more accurate forest height results using SAR interferometry. Low wavelength band SAR images (X-band) should be used as the satellite signal do not penetrate the canopy. Hence backscatter contribution will consist of only surface backscatters from the top forest canopy as opposed to volume scattering by larger wavelength bands (C, L and P).
- Temporal decorrelation can be reduced by taking images acquired in a very short time interval to maximise retrieval of high coherence in forest areas which results in high accurate interferometric results. This can be achieved by employing SAR satellite system which co-fly in close information or satellite in bistatic mode (Fu *et al.*, 2014).

On SAR tomography analysis

- A sufficient number of images should be acquired to establish a required baseline for vertical retrieval of backscatter values for AGB estimation.

LIST OF REFERENCES

- Ager, T. P. (2011). An introduction to synthetic aperture radar imaging. *Oceanography*, 24(3), 162–173. <https://doi.org/10.5670/oceanog.2011.65>.
- Antropov, O., Rauste, Y., Häme, T., & Praks, J. (2017). Polarimetric ALOS PALSAR time series in mapping biomass of boreal forests. *Remote Sensing*, 9(10), 1–24. <https://doi.org/10.3390/rs9100999>.
- Asner, G. P. (2001). Cloud cover in Landsat observations of the Brazilian Amazon. *International Journal of Remote Sensing*, 22(18), 3855–3862. <https://doi.org/10.1080/01431160010006926>.
- Brown, S. (2002). Measuring carbon in forests: Current status and future challenges. *Environmental Pollution*, 116(3), 363–372. [https://doi.org/10.1016/S0269-7491\(01\)00212-3](https://doi.org/10.1016/S0269-7491(01)00212-3).
- Caicoya, A. T., Kugler, F., Pardini, M., Hajnsek, I., & Papathanassiou, K. (2015). Forest Biomass Estimation from SAR Vertical Reflectivity Profiles. *7th International Workshop on Science and Applications of SAR Polarimetry and Polarimetric Interferometry*, 12(12), 2379–2383. <https://doi.org/10.1109/LGRS.2015.2477858>.
- Carver, K. (1988). “SAR Synthetic Aperture Radar – Earth Observing System.” NASA National Aeronautics & Space Administration. Instrument Panel Report. Vol IIf. Radar Imaging From Space. 233 pp.
- Chave, J., Réjou-Méchain, M., Búrquez, A., Chidumayo, E., Colgan, M. S., Delitti, W. B. C., Vieilledent, G. (2014). Improved allometric models to estimate the aboveground biomass of tropical trees. *Global Change Biology*, 20(10), 3177–3190. <https://doi.org/10.1111/gcb.12629>.
- Chehade, B. E. H., Ferro-Famil, L., Dinh, H. T. M., Toan, T. Le, & Tebaldini, S. (2016). Tropical forest biomass retrieval using P-band Pol/TomSAR data, 1–4. Retrieved from <https://hal.archives-ouvertes.fr/hal-01403177>.
- Cloude, S. R. (2005). Pol-InSAR training course. Cupar: Esa. Retrieved from https://earth.esa.int/documents/653194/656796/Pol-InSAR_Training_Course.pdf.
- Cloude, S. R. (2006). Polarization coherence tomography (PCT): A tutorial introduction. Cupar: Esa. Retrieved from https://earth.esa.int/documents/653194/656796/PCT_Training_Course.pdf.
- Cloude, S. R. (2007). Dual-baseline coherence tomography. *IEEE Geoscience and Remote Sensing Letters*, 4(1), 127–131. <https://doi.org/10.1109/LGRS.2006.885893>.
- Cloude, S. R., & Papathanassiou, K. P. (1998). Polarimetric SAR Interferometry. *IEEE Transactions on Geoscience and Remote Sensing*, 36(5), 1551–1565. <https://doi.org/10.1109/36.718859>.
- Djomo, A. N., & Chimi, C. D. (2017). Tree allometric equations for estimation of above, below and total biomass in a tropical moist forest: Case study with application to remote sensing. *Forest Ecology and Management*, 391, 184–193. <https://doi.org/10.1016/j.foreco.2017.02.022>.
- Du, H., Zhou, G., Ge, H., Fan, W., Xu, X., Fan, W., & Shi, Y. (2012). Satellite-based carbon stock estimation for bamboo forest with a non-linear partial least square regression technique. *International Journal of Remote Sensing*, 33(6), 1917–1933. <https://doi.org/10.1080/01431161.2011.603379>.
- Dube, T., & Mutanga, O. (2015). Evaluating the utility of the medium-spatial resolution Landsat 8 multispectral sensor in quantifying aboveground biomass in uMgeni catchment, South Africa. *ISPRS Journal of Photogrammetry and Remote Sensing*, 101, 36–46. <https://doi.org/10.1016/j.isprsjprs.2014.11.001>.
- Estornell, J., Ruiz, L. A., Velázquez-Martí, B., & Fernández-Sarría, A. (2011). Estimation of shrub biomass by

- airborne LiDAR data in small forest stands. *Forest Ecology and Management*, 262(9), 1697–1703. <https://doi.org/10.1016/j.foreco.2011.07.026>.
- Fan, S., Gloor, M., Mahlman, J., Pacala, S., Sarmiento, J., Takahashi, T., & Tans, P. (1998). A large terrestrial carbon sink in North America implied by atmospheric and oceanic carbon dioxide data and models. *Science*, 282(5388), 442–446. <https://doi.org/10.1126/science.282.5388.442>.
- FAO. (2017). What is REDD+? Retrieved May 29, 2017, from <http://www.unredd.net/about/what-is-redd-plus.html>.
- FAO Climate Energy and Tenure Division. (2009). *BIOMASS - Assessment of the status of the development of the standards for the terrestrial essential climate variables*. (FAO, Ed.). Rome, Italy: FAO. Retrieved from <http://www.fao.org/3/a-i1238e.pdf>.
- Food and Agriculture Organization of the United Nations. (2005). *Global Forest Resources Assessment 2005 Progress towards sustainable forest management*. Retrieved from <ftp://ftp.fao.org/docrep/fao/008/A0400E/A0400E00.pdf>.
- Fu, W. X., Guo, H. D., Xie, C., Lu, Y. C., & Li, X. W. (2014). Forest height inversion using dual-pol polarimetric SAR interferometry. *IOP Conference Series: Earth and Environmental Science*, 17(1). <https://doi.org/10.1088/1755-1315/17/1/012072>.
- Ghasemi, N., Sahebi, M. R., & Mohammadzadeh, A. (2011). A review on biomass estimation methods using synthetic aperture radar data. *International Journal Ofgeomatics and Geosciences*, 1(4), 776–788.
- Gibbs, H. K., Brown, S., Niles, J. O., & Foley, J. A. (2007). Monitoring and estimating tropical forest carbon stocks: making REDD a reality. *Environmental Research Letters*, 2(2007), 45023. <https://doi.org/10.1088/1748-9326/2/4/045023>.
- Gobakken, T., & Næsset, E. (2008). Assessing effects of laser point density, ground sampling intensity, and field sample plot size on biophysical stand properties derived from airborne laser scanner data. *Canadian Journal of Forest Research*, 38(5), 1095–1109. <https://doi.org/10.1139/X07-219>.
- Hamdan, O., Mohd Hasmadi, I., Khali Aziz, H., Norizah, K., & Helmi Zuhaidi, M. S. (2015). L-band saturation level for aboveground biomass of dipterocarp forests in peninsular Malaysia. *Journal of Tropical Forest Science*, 27(3), 388–399.
- Hertz, H. (2008). Overview of Polarimetric Radar Imaging. In *Polarimetric Radar Imaging* (1st ed., p. 432). Taylor & Francis Group, LLC.
- Hirata Y, Takao G, Sato, T., & Toriyama, J. (2012). (2012). *REDD+ Cookbook: How to measure and monitor forest carbon*. Japan: FFPRI REDD Research and Development Center, Japan. Retrieved from <https://www.ffpri.affrc.go.jp/redd-rdc/en/reference/cookbook.html> 155pp.
- Ho Tong Minh, D., Le Toan, T., Rocca, F., Tebaldini, S., Mariotti, M., & Villard, L. (2014). Relating P-Band Synthetic Aperture Radar Tomography to Tropical Forest Biomass. *Ieee Transactions on Geoscience and Remote Sensing*, 52(2). <https://doi.org/10.1109/TGRS.2013.2246170>
- Ho Tong Minh, D., Le Toan, T., Rocca, F., Tebaldini, S., Villard, L., Réjou-Méchain, M., Chave, J. (2016). SAR tomography for the retrieval of forest biomass and height: Cross-validation at two tropical forest sites in French Guiana. *Remote Sensing of Environment*, 175, 138–147. <https://doi.org/10.1016/j.rse.2015.12.037>
- Ho Tong Minh, D., Tebaldini, S., Rocca, F., Le Toan, T., Villard, L., & Dubois-Fernandez, P. C. (2015). Capabilities of BIOMASS tomography for investigating tropical forests. *IEEE Transactions on Geoscience and Remote Sensing*, 53(2), 965–975. <https://doi.org/10.1109/TGRS.2014.2331142>.
- Hong Tong Minh, D., Rocca, F., Tebaldini, S., Alessandro, M. M., Toan, T. Le, & Villard, L. (2012). Relating

- Tropical Forest Biomass to P-band SAR Tomography. *IEEE International Geoscience and Remote Sensing Symposium (IGARSS)*, 7589–7592. Retrieved from http://ieeexplore.ieee.org/xpls/abs_all.jsp?arnumber=6351871.
- Hosoi, F., Nakai, Y., & Omasa, K. (2013). 3-D voxel-based solid modeling of a broad-leaved tree for accurate volume estimation using portable scanning lidar. *ISPRS Journal of Photogrammetry and Remote Sensing*, 82, 41–48. <https://doi.org/10.1016/j.isprsjprs.2013.04.011>.
- Hounsfield, G. N. (1979). Computed Medical Imaging, 19. Retrieved from https://www.nobelprize.org/nobel_prizes/medicine/laureates/1979/hounsfield-lecture.pdf.
- Hurtado, D. M. (2012). *Interferometric Processing of TanDEM-X Images for Forest Height Estimation*. Aalto University.
- Husin, M. Z., & Rajpar, M. N. (2015). Effects of logging and recovery process on avian richness and diversity in hill dipterocarp tropical rainforest-Malaysia. *Journal of Environmental Biology*, 36(January), 121–127.
- Hyde, P., Nelson, R., Kimes, D., & Levine, E. (2007). Exploring LiDAR–RaDAR synergy—predicting aboveground biomass in a southwestern ponderosa pine forest using LiDAR, SAR and InSAR. *Remote Sensing of Environment*, 106(1), 28–38. <https://doi.org/10.1016/j.rse.2006.07.017>.
- Hyypä, J., Hyypä, H., Leckie, D., Gougeon, F., Yu, X., & Maltamo, M. (2008). Review of methods of small footprint airborne laser scanning for extracting forest inventory data in boreal forests. *International Journal of Remote Sensing*, 29(5), 1339–1366. <https://doi.org/10.1080/01431160701736489>.
- Imhoff, M. L. (1995). Radar backscatter and biomass saturation: ramifications for global biomass inventory. *IEEE Transactions on Geoscience and Remote Sensing*, 33(2), 511–518. <https://doi.org/10.1109/36.377953>.
- Joshi, N., Mitchard, E., Schumacher, J., Johannsen, V., Saatchi, S., & Fensholt, R. (2015). L-Band SAR Backscatter Related to Forest Cover, Height and Aboveground Biomass at Multiple Spatial Scales across Denmark. *Remote Sensing*, 7(4), 4442–4472. <https://doi.org/10.3390/rs70404442>.
- Joshi, S. K., & Kumar, S. (2017). Spaceborne PolInSAR tomography for vertical profile retrieval of forest vegetation. *Journal of Applied Remote Sensing*, 11(1), 16001. <https://doi.org/10.1117/1.JRS.11.016001>.
- Kaasalainen, S., Holopainen, M., Karjalainen, M., Vastaranta, M., Kankare, V., Karila, K., & Osmanoglu, B. (2015). Combining lidar and synthetic aperture radar data to estimate forest biomass: Status and prospects. *Forests*, 6(1), 252–270. <https://doi.org/10.3390/f6010252>.
- Kaasalainen, S., Krooks, A., Liski, J., Raunonen, P., Kaartinen, H., Kaasalainen, M., Mäkipää, R. (2014). Change detection of tree biomass with terrestrial laser scanning and quantitative structure modelling. *Remote Sensing*, 6(5), 3906–3922. <https://doi.org/10.3390/rs6053906>.
- Kershaw, J. A., Ducey, M. J., Beers, T. W., & Husch, B. (2016). *Forest mensuration* (5th ed.). New York: John Wiley . Retrieved from <http://ezproxy.utwente.nl:2200/patron/FullRecord.aspx?p=4731589>.
- Kumar, S., Khatri, U. G., Chandola, S., Agrawal, S., & Kushwaha, S. P. S. (2017). Polarimetric SAR Interferometry based modeling for tree height and aboveground biomass retrieval in a tropical deciduous forest. *Advances in Space Research*, 60(3), 571–586. <https://doi.org/10.1016/j.asr.2017.04.018>.
- Laar, A. van, & Akça, A. (2007). *Forest Mensuration* (Vol. 13). Dordrecht: Springer Netherlands. <https://doi.org/10.1126/science.24.624.760>.
- Lazeký, M., Çomut, F. C., Hlaváčová, I., & Gürboğa, Ş. (2015). Practical Application of Satellite-Based SAR Interferometry for the Detection of Landslide Activity. *Procedia Earth and Planetary Science*, 15, 613–618. <https://doi.org/10.1016/j.proeps.2015.08.113>.
- Le Toan, T., Quegan, S., Woodward, I., Lomas, M., Delbart, N., & Picard, G. (2004). Relating radar remote

- sensing of biomass to modelling of forest carbon budgets. *Climatic Change*, 67(2–3), 379–402. <https://doi.org/10.1007/s10584-004-3155-5>.
- Lee, J.-S., & Pottier, E. (2009). Selected polarimetric SAR applications. *Polarimetric Radar Imaging: From Basics to Applications*, 1–56.
- Lee, S., Kugler, F., Papathanassiou, K. P., Member, S., & Hajnsek, I. (2013). Quantification of Temporal Decorrelation Effects at L-Band for Polarimetric SAR Interferometry Applications, 6(3), 1351–1367.
- Lei, Y., & Siqueira, P. (2014). Estimation of forest height using spaceborne repeat-pass L-band InSAR correlation magnitude over the US state of Maine. *Remote Sensing*, 6(11), 10252–10285. <https://doi.org/10.3390/rs61110252>.
- Li, L., Chen, E., Li, Z., Feng, Q., Zhao, L., & Yang, W. (2015). DEM and DHM reconstruction in tropical forests: Tomographic results at P-band with three flight tracks. *International Geoscience and Remote Sensing Symposium (IGARSS), 2015–Novem*, 3018–3021. <https://doi.org/10.1109/IGARSS.2015.7326451>.
- Li, W., Chen, E., Li, Z., Ke, Y., & Zhan, W. (2015). Forest aboveground biomass estimation using polarization coherence tomography and PolSAR segmentation. *International Journal of Remote Sensing*, 36(2), 530–550. <https://doi.org/10.1080/01431161.2014.999383>.
- Liang, X., Kankare, V., Hyypää, J., Wang, Y., Kukko, A., Haggrén, H., ... Vastaranta, M. (2016). Terrestrial laser scanning in forest inventories. *ISPRS Journal of Photogrammetry and Remote Sensing*, 115, 63–77. <https://doi.org/10.1016/j.isprsjprs.2016.01.006>.
- Lombardini, F., Cai, F., & Pasculli, D. (2013). Spaceborne 3-D SAR Tomography for Analyzing Garbled Urban Scenarios : Single-Look Superresolution Advances and Experiments, 6(2), 960–968.
- Lombardini, F., & Pardini, M. (2008). 3-D SAR tomography: The multibaseline sector interpolation approach. *IEEE Geoscience and Remote Sensing Letters*, 5(4), 630–634. <https://doi.org/10.1109/LGRS.2008.2001283>.
- Lombardini, F., & Reigber, A. (2014). Adaptive Spectral Estimation for Multibaseline SAR Tomography with Airborne L-band Data, 0(C), 2014–2016.
- Lombardini, F., & Viviani, F. (2014). Multidimensional SAR Tomography : Advances for Urban and Prospects for Forest / Ice Applications, 225–228.
- Lu, D., Mausel, P., Brondízio, E., & Moran, E. (2004). Relationships between forest stand parameters and Landsat TM spectral responses in the Brazilian Amazon Basin. *Forest Ecology and Management*, 198(1–3), 149–167. <https://doi.org/10.1016/j.foreco.2004.03.048>.
- Lucas, R. M., Mitchell, A. L., & Armston, J. (2015). Measurement of Forest Above-Ground Biomass Using Active and Passive Remote Sensing at Large (Subnational to Global) Scales. *Current Forestry Reports*, 1(3), 162–177. <https://doi.org/10.1007/s40725-015-0021-9>.
- Luo, S., Wang, C., Xi, X., Pan, F., Peng, D., Zou, J., ... Qin, H. (2017). Fusion of airborne LiDAR data and hyperspectral imagery for aboveground and belowground forest biomass estimation. *Ecological Indicators*. <https://doi.org/10.1016/j.ecolind.2016.10.001>.
- Malaysian Meteorological Department. (2017). Malaysia's Climate. Retrieved June 7, 2017, from <http://www.met.gov.my/in/web/metmalaysia/climate/generalinformation/malaysia>.
- Malhi, Y., Baldocchi, D. D., & Jarvis, P. G. (1999). The carbon balance of tropical, temperate and boreal forests. *Plant, Cell and Environment*, 22(6), 715–740. <https://doi.org/10.1046/j.1365-3040.1999.00453.x>.
- Martin Bélanda, Jean-Luc Widlowskib, Richard A. Fourniera, Jean-François Côtéa, M. M. V. (2011). Estimating leaf area distribution in savanna trees from terrestrial LiDAR measurements. *Agricultural and Forest Meteorology*, 151(9), 1252–1266. <https://doi.org/10.1016/j.agrformet.2011.05.004>.

- Mengesha, T., Hawkins, M., & Nieuwenhuis, M. (2015). Validation of terrestrial laser scanning data using conventional forest inventory methods. *European Journal of Forest Research*, 134(2), 211–222. <https://doi.org/10.1007/s10342-014-0844-0>.
- Mermoz, S., M. Réjou-Méchain, L. Villard, T. Le Toan, V. Rossi, S. G.-F. (2014). Biomass of Dense Forests Related to L-band SAR Backscatter? *IEEE International Geoscience and Remote Sensing Symposium (IGARSS)*, (May), 2011–2014.
- Mermoz, S., Réjou-Méchain, M., Villard, L., Le Toan, T., Rossi, V., & Gourlet-Fleury, S. (2015). Decrease of L-band SAR backscatter with biomass of dense forests. *Remote Sensing of Environment*, 159, 307–317. <https://doi.org/10.1016/j.rse.2014.12.019>.
- Moreira, A., Prats, P., Younis, M., Krieger, G., Hajnsek, I., & Papathanassiou, K. (2013). A Tutorial on Synthetic Aperture Radar. *IEEE Geoscience and Remote Sensing Magazine*, (march), 1–43. <https://doi.org/10.1109/MGRS.2013.2248301>.
- Neumann, M., Saatchi, S. S., Ulander, L. M. H., & Fransson, J. E. S. (2012). Assessing Performance of L- and P-Band Polarimetric Interferometric SAR Data in Estimating, 50(3), 714–726.
- Odipo, V., Nickless, A., Berger, C., Baade, J., Urbazaev, M., Walther, C., & Schmullius, C. (2016). Assessment of Aboveground Woody Biomass Dynamics Using Terrestrial Laser Scanner and L-Band ALOS PALSAR Data in South African Savanna. *Forests*, 7(12), 294. <https://doi.org/10.3390/f7120294>.
- Omar, H., Ismail, M. H., Hamzah, K. A., Shafri, H. Z. M., & Kamarudin, N. (2015). Estimating biomass in logged tropical forest using L-band SAR (PALSAR) data and GIS. *Sains Malaysiana*, 44(8), 1085–1093. <https://doi.org/10.17576/jsm-2015-4408-02>.
- Paris, C., Kelbe, D., Aardt, J. Van, & Bruzzone, L. (2015). A Precise Estimate of the 3D Structure of the Forest Based on the Fusion of Airborne and Terrestrial Lidar Data. *IEEE International Geoscience and Remote Sensing Symposium (IGARSS)*, 49–52.
- Powell, S. L., Cohen, W. B., Healey, S. P., Kennedy, R. E., Moisen, G. G., Pierce, K. B., & Ohmann, J. L. (2010). Quantification of live aboveground forest biomass dynamics with Landsat time-series and field inventory data: A comparison of empirical modeling approaches. *Remote Sensing of Environment*, 114(5), 1053–1068. <https://doi.org/10.1016/j.rse.2009.12.018>.
- Rahman, M. Z. A., Bakar, M. A. A., Razak, K. A., Rasib, A. W., Kanniah, K. D., Kadir, W. H. W., Latif, Z. A. (2017). Non-destructive, laser-based individual tree aboveground biomass estimation in a tropical rainforest. *Forests*, 8(3). <https://doi.org/10.3390/f8030086>.
- Rajpar, M. N., & Zakaria, M. (2014). Assessing the Effects of Logging Activities on Avian Richness and Diversity in Different Aged Post-Harvested Hill Dipterocarp Tropical Rainforest of Malaysia. *American Journal of Applied Sciences*, 11(9), 1519–1529. <https://doi.org/10.3844/ajassp.2014.1519.1529>.
- Reigber, a., & Moreira, a. (2000). First demonstration of airborne SAR tomography using multibaseline L-band data. *IEEE Transactions on Geoscience and Remote Sensing*, 38(5), 2142–2152. <https://doi.org/10.1109/36.868873>.
- Ruiz, L. A., Hermosilla, T., Mauro, F., & Godino, M. (2014). Analysis of the influence of plot size and LiDAR density on forest structure attribute estimates. *Forests*, 5(5), 936–951. <https://doi.org/10.3390/f5050936>.
- Sai Bharadwaj, P., Kumar, S., Kushwaha, S. P. S., & Bijker, W. (2015). Polarimetric scattering model for estimation of above ground biomass of multilayer vegetation using ALOS-PALSAR quad-pol data. *Physics and Chemistry of the Earth*, 83–84, 187–195. <https://doi.org/10.1016/j.pce.2015.09.003>.
- Sarker, M. L. R., Nichol, J., Ahmad, B., Busu, I., & Rahman, A. A. (2012). Potential of texture measurements

- of two-date dual polarization PALSAR data for the improvement of forest biomass estimation. *ISPRS Journal of Photogrammetry and Remote Sensing*, 69, 146–166. <https://doi.org/10.1016/j.isprsjprs.2012.03.002>.
- Seidel, D., Albert, K., Fehrmann, L., & Ammer, C. (2012). The potential of terrestrial laser scanning for the estimation of understory biomass in coppice-with-standard systems. *Biomass and Bioenergy*, 47, 20–25. <https://doi.org/10.1016/j.biombioe.2012.10.009>.
- Shimada, M., Isoguchi, O., Tadono, T., & Isono, K. (2009). PALSAR radiometric and geometric calibration. *IEEE Transactions on Geoscience and Remote Sensing*, 47(12), 3915–3932. <https://doi.org/10.1109/TGRS.2009.2023909>.
- Srinivasan, S., Popescu, S. C., Eriksson, M., Sheridan, R. D., & Ku, N. W. (2015). Terrestrial laser scanning as an effective tool to retrieve tree level height, crown width, and stem diameter. *Remote Sensing*, 7(2), 1877–1896. <https://doi.org/10.3390/rs70201877>.
- Stefano Tebaldini, Mauro Mariotti D' Alessandro, H. T. M. D. and F. R. (2011). P Band Penetration in Tropical and Boreal Forests: Tomographical Results. In *Proc. IEEE Geoscience and Remote Sensing Symposium* (pp. 4241–4244).
- Sterenczak, K., Zasada, M., & Brach, M. (2013). The Accuracy Assessment of DTM Generated from LIDAR Data for Forest Area – a Case Study for Scots Pine Stands in Poland. *Baltic Forestry*, 252–262.
- Strahler, A. H., Jupp, D. L. B., Woodcock, C. E., Schaaf, C. B., Yao, T., Zhao, F., Boykin-Morris, W. (2008). Retrieval of forest structural parameters using a ground-based lidar instrument (Echidna®). *Canadian Journal of Remote Sensing*, 34(SUPPL. 2). <https://doi.org/10.5589/m08-046>.
- Sumareke, A. M. (2016). *Modelling and Mapping Aboveground Biomass and Carbon Stock Using Alos-2 Palsar-2 Data in Ayer Hitam Tropical Rainforest Reserve in Malaysia (Msc thesis)*. University of Twente Faculty of Geo_Information and Earth Observation(ITC), Enschede, Netherlands.
- Suzuki, R., Kim, Y., & Ishii, R. (2013). Sensitivity of the backscatter intensity of ALOS/PALSAR to the above-ground biomass and other biophysical parameters of boreal forest in Alaska. *Polar Science*, 7(2), 100–112. <https://doi.org/10.1016/j.polar.2013.03.001>.
- Tebaldini, S. (2010). Single and multipolarimetric SAR tomography of forested areas: A parametric approach. *IEEE Transactions on Geoscience and Remote Sensing*, 48(5), 2375–2387. <https://doi.org/10.1109/TGRS.2009.2037748>.
- Tebaldini, S., & Rocca, F. (2012). Multibaseline polarimetric SAR tomography of a boreal forest at P- and L-Bands. *IEEE Transactions on Geoscience and Remote Sensing*, 50(1), 232–246. <https://doi.org/10.1109/TGRS.2011.2159614>.
- The REDD Desk. (2017). Tanzania | The REDD Desk. Retrieved June 13, 2017, from <http://theredddesk.org/countries/tanzania>.
- Toan, T. Le, Ulander, L., Papathanassiou, K., & Rocca, F. (2013). Status of the retrieval algorithms of the Biomass mission. In *The 6th International Workshop on Science and Applications of SAR Polarimetry and Polarimetric Interferometry* (p. 30). Rome, Italy: European Space Agency. Retrieved from https://earth.esa.int/c/document_library/get_file?folderId=408743&name=DLFE-5545.pdf.
- Urasawa, F., Yamada, H., Yamaguchi, Y., & Sato, R. (2016). Fundamental study on multi-baseline SAR tomography by Pi-SAR-L2. In *2016 URSI Asia-Pacific Radio Science Conference (URSI AP-RASC)* (pp. 514–515). IEEE. <https://doi.org/10.1109/URSIAP-RASC.2016.7601342>.
- Van Laar, A., & Akca, A. (2007). *Forest Mensuration*. Springer (Vol. 13). Dordrecht: Springer Netherlands. <https://doi.org/10.1126/science.24.624.760>.
- van Leeuwen, M., & Nieuwenhuis, M. (2010). Retrieval of forest structural parameters using LiDAR remote

- sensing. *European Journal of Forest Research*, 129(4), 749–770. <https://doi.org/10.1007/s10342-010-0381-4>.
- Villard, L., Le Toan, T., Ho Tong Minh, D., Mermoz, S., & Bouvet, A. (2016). Forest Biomass From Radar Remote Sensing. *Land Surface Remote Sensing in Agriculture and Forest*, 363–425. <https://doi.org/10.1016/B978-1-78548-103-1.50009-1>.
- Yu, Y., & Saatchi, S. (2016). Sensitivity of L-band SAR backscatter to aboveground biomass of global forests. *Remote Sensing*, 8(6). <https://doi.org/10.3390/rs8060522>.
- World Weather and Climate Information (2016). Retrieved February 10, 2018 from <https://weather-and-climate.com/average-monthly-Rainfall-Temperature-Sunshine,Kuantan,Malaysia>.
- Zawawi, A. A., Shiba, M., & Jemali, N. J. N. (2015). Accuracy of LiDAR-based tree height estimation and crown recognition in a subtropical evergreen broad-leaved forest in Okinawa, Japan. *Forest Systems*, 24(1), 1–11. <https://doi.org/10.5424/fs/2015241-05476>.
- Zhou, X., Chang, N.-B., & Li, S. (2009). Applications of SAR Interferometry in Earth and Environmental Science Research. *Sensors*, 9(3), 1876–1912. <https://doi.org/10.3390/s90301876>.
- Zhu, X. X., Member, S., & Bamler, R. (2010). Very High Resolution Spaceborne SAR Tomography in Urban Environment. *IEEE Transactions on Geoscience and Remote Sensing*, 48(12), 4296–4308.

APPENDICES

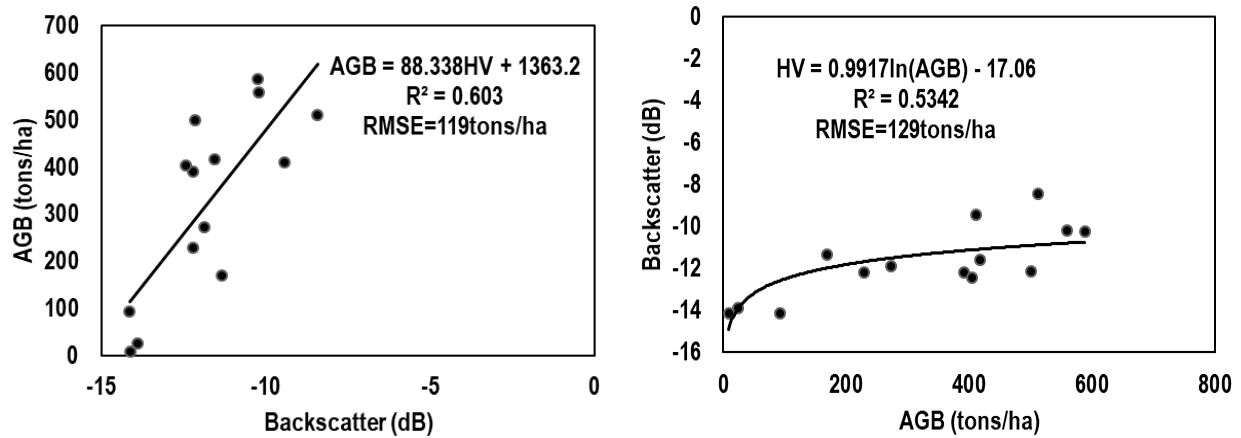
Appendix 1: Field data collection sheet

Multiple R	0.876843
R Square	0.768854
Adjusted R Square	0.749592
Standard Error	97.70343
Observations	14

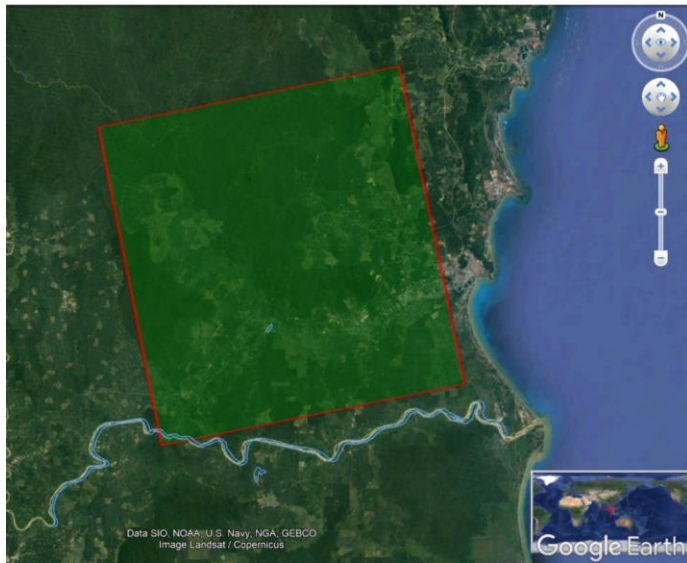
ANOVA					
	<i>df</i>	<i>SS</i>	<i>MS</i>	<i>F</i>	<i>Significance_F</i>
Regression	1	381028.7	381028.7	39.91517	3.84E-05
Residual	12	114551.5	9545.961		
Total	13	495580.2			

	<i>Coefficients</i>	<i>Standard_Error</i>	<i>t_Stat</i>	<i>P-value</i>
Intercept	1207.132	141.7414	8.516439	1.97E-06
HV_2016	69.84126	11.0546	6.317846	3.84E-05

Appendix 3: Results of the linear and logarithmic regression between AGB and HV backscatter for the 28 January 2017 backscatter image.

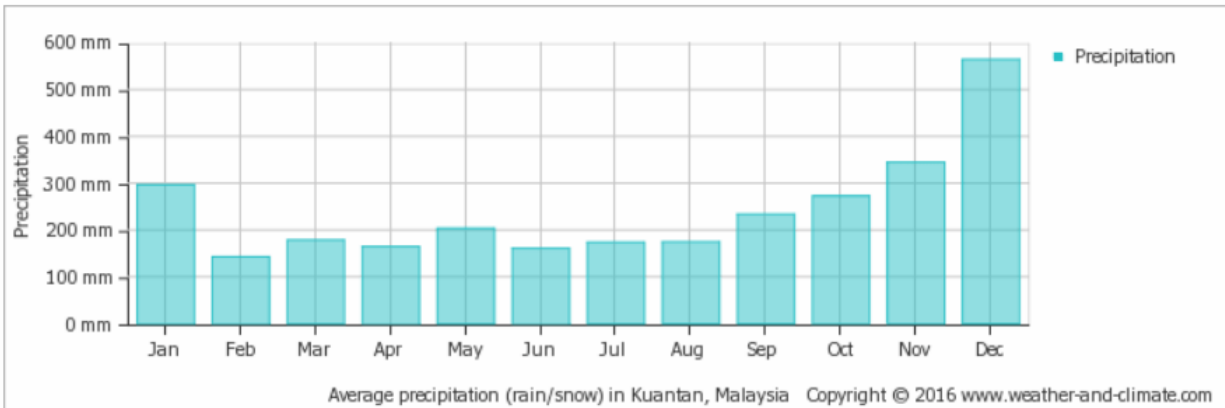


Appendix 4: ALOS-2 PALSAR-2 SAR image footprint as viewed in Google Earth



Appendix 5: Average monthly rainfall pattern over the year in Kuantan, Malaysia

(source: <https://weather-and-climate.com/average-monthly-Rainfall-Temperature-Sunshine,Kuantan,Malaysia>)



Appendix 6: Backscatter images of September 2016, January 2017 and September 2017 for Berkelah tropical rain forest, Malaysia

